

A Unified Understanding of the Experimental Controlling of the T_c of Bilayer Nickelates

Zeyu Chen,^{1,*} Jia-Heng Ji,^{1,*} Yu-Bo Liu,^{2,*} Ming Zhang,³ and Fan Yang^{1,†}

¹*School of Physics, Beijing Institute of Technology, Beijing 100081, China*

²*Institute of Theoretical Physics, Chinese Academy of Sciences, Beijing 100190, China*

³*Zhejiang Key Laboratory of Quantum State Control and Optical Field Manipulation, Department of Physics, Zhejiang Sci-Tech University, 310018 Hangzhou, China*

Recently, a series of experiments which control the T_c of the bilayer nickelates $\text{La}_3\text{Ni}_2\text{O}_7$ through varying environmental conditions, including the rare-earth Sm/Nd substitution, the pressure on the bulk material, the compressive strain on the film and the hole doping through over-oxidation or alkaline earth element substitution have caught great interests. Here, we provide a unified understanding toward all these experiments based on the minimal single $d_{x^2-y^2}$ -orbital bilayer $t - J_{\parallel} - J_{\perp}$ model proposed previously. With model parameters input from density-functional-theoretical calculations under varying experimental conditions, we adopt combined slave-boson-mean-field and density-matrix-renormalization-group approaches to solve the model and compare with experiments. Our results yield that, the bulk T_c under pressure enhances with the Sm/Nd substitution fraction, the bulk T_c -pressure relation takes a dome shaped curve, the T_c of the thin film enhances with compressive strain. The obtained parameters dependence of T_c in these three experiments mainly originates from the variation of J_{\perp} with experimental conditions. As for the hole doping, our results provide that T_c decreases with the hole doping level δ , due to reduced density of state for the $d_{x^2-y^2}$ -orbital. All these results are qualitatively consistent with experiments. We further conduct a comparative weak-coupling random-phase-approximation (RPA) based study on these experiments and find that our strong-coupling $t - J_{\parallel} - J_{\perp}$ model provides a more natural understanding of the experiments. We propose that electron doping implemented through substitution of La by element with higher valence, or further enhancement of the compressive strain in the film, can enhance T_c .

I. INTRODUCTION

The discovery of superconductivity (SC) with critical temperature T_c above the boiling point of liquid nitrogen in $\text{La}_3\text{Ni}_2\text{O}_7$ under high pressure (HP) [1] has aroused a surge in the exploration of Ruddlesden-Popper (RP) phase nickelate superconductors [2–10], which has driven the discovery of SC in pressurized $\text{La}_4\text{Ni}_3\text{O}_{10}$ [11–13], $\text{La}_5\text{Ni}_3\text{O}_{11}$ [14] and $\text{La}_6\text{Ni}_4\text{O}_{14}$ [15, 16], catching great research interests [17–81]. More recently, SC with T_c above the McMillan limit has been detected in the film of $\text{La}_3\text{Ni}_2\text{O}_7$ at ambient pressure (AP) [82], allowing various experimental detections in this family to explore their pairing mechanism and physical properties [83–98]. The RP-phase nickelates have become a new platform for the realization of the SC with high T_c besides the cuprates and iron-pnictides. Currently, while the pairing mechanism of the SC with high T_c in the RP-phase nickelates still remains elusive, a particularly important related question is: what is the crucial ingredient which affects the T_c , and how to enhance the T_c ?

The $\text{La}_3\text{Ni}_2\text{O}_7$ hosts a quasi-2D structure with each unit cell consisting of two NiO_2 layer hybridized via the Ni-O-Ni bonding [1]. First-principle density-functional-theory (DFT) based calculations suggest that the low-energy degrees of freedom in the material are dominated by the nearly half-filled Ni-3d_{z^2} orbital and the

nearly quarter-filled $\text{Ni-3d}_{x^2-y^2}$ orbital [33], implying strong electron correlations. On the one hand, while the ultrafast dynamics experiment reveals weak electron-phonon coupling (EPC) in $\text{La}_3\text{Ni}_2\text{O}_7$ [23], the DFT calculation suggests that the EPC cannot explain the SC with high T_c in $\text{La}_3\text{Ni}_2\text{O}_7$ [71, 99]. On the other hand, the orbital-selective strong band renormalization observed by the angle-resolved photoemission spectrum (ARPES) [26, 27], the strongly reduced electronic kinetic energy detected by the optical conductivity [24], and the strange-metal behavior revealed by the transport experiment combinedly suggest strong electron correlation in the system [2], implying an electron-electron (e-e) interaction driven pairing mechanism. Furthermore, proximity between the SC with high T_c and the spin density wave (SDW) [17, 18, 21, 29, 30, 32, 100–102] in the pressure vs. temperature phase diagram suggests that the pairing mechanism might be closely related to magnetically originating interactions.

In the framework of e-e interaction driven pairing mechanism, the existing theories are divided into weak-coupling theories and strong-coupling ones. Weak-coupling theories start from the DFT band structure equipped with standard multi-orbital Hubbard-Kanamori interaction, and adopt such perturbative approaches as the functional renormalization group (FRG) [35, 47, 103–105], the random-phase-approximation (RPA) [44, 51, 62, 106–108] and the fluctuation-exchange [46, 109] to reveal that the spin fluctuations in the system mediate the s^{\pm} -wave pairing. Generally in such theories, details of band structure near the

* These authors contributed equally to this work.

† yangfan_blg@bit.edu.cn

Fermi surface (FS), such as the density of state (DOS) and the FS-nesting, are crucial in determining the pairing symmetry and T_c . Strong-coupling theories work in the large- U limit, under which different forms of low-energy effective models are proposed, in which different forms of effective superexchange interactions provide the pairing interaction. Although the interplay of the two Ni-3d E_g orbitals are generally important in these strong-coupling theories, these theories can be further divided into the $d_{x^2-y^2}$ -orbital dominated pairing theories [37, 38, 49, 52, 55, 56, 59, 64, 68, 69, 110–117] and the d_{z^2} -orbital dominated pairing ones [41–43, 61, 65]. Presently, it is unclear which type of theories are more relevant to the real materials of $\text{La}_3\text{Ni}_2\text{O}_7$.

Various experiments have been done to control the T_c of $\text{La}_3\text{Ni}_2\text{O}_7$. For bulk material of $\text{La}_3\text{Ni}_2\text{O}_7$ at HP, the strength of the imposed pressure and the rare-earth element substitution of La can obviously influence the T_c . The pressure-dependence of T_c exhibits a right-triangle shaped curve [8, 102]: With the enhancement of the pressure, the T_c first abruptly enhances to its maximum near 18GPa, and then gradually decreases. Through partially substituting La by Sm [96, 98] or Nd [97] in $\text{La}_3\text{Ni}_2\text{O}_7$, the T_c can be enhanced to 96 K or 98 K. In the thin film of $\text{La}_3\text{Ni}_2\text{O}_7$ at AP, the strain and hole doping can obviously affect the T_c . Experiments for the $\text{La}_3\text{Ni}_2\text{O}_7$ thin film grown on various different substrates show that compressive strain enhances T_c , while tensile strain suppresses T_c [82]. Recent experiments on the $\text{La}_3\text{Ni}_2\text{O}_7$ thin film shows that over-oxidization [118, 119] or alkaline earth element substitution [90, 119] will obviously suppress T_c , suggesting that hole doping suppresses the T_c . These experiments set constraint for theoretical models and provide insight for the establishment of relevant theories for the pairing mechanism of $\text{La}_3\text{Ni}_2\text{O}_7$.

In this paper, we provide a unified understanding of all the experiments introduced above, based on one minimal model. We hold that the nearly half-filled d_{z^2} orbital mainly acts like a localized spin, while the nearly quarter-filled $d_{x^2-y^2}$ orbital dominantly carries SC, with a pairing mechanism driven by the effective interlayer superexchange interaction transmitted from the d_{z^2} orbital through the strong Hund's rule coupling [37, 49, 55, 68]. Based on this point of view, we adopt the single $d_{x^2-y^2}$ -orbital bilayer $t - J_{\parallel} - J_{\perp}$ model [37, 38, 49, 55, 56, 59, 69, 110–112, 115–117, 120, 121] proposed previously by part of the authors. This model exhibits an interlayer s-wave pairing, whose T_c mainly benefits from two factors: increased interlayer superexchange J_{\perp} which favors pairing and increased filling fraction which enhances the DOS. With model parameters input from DFT calculations under different experimental conditions, we solve the model via combined slave-boson-mean-field (SBMF) and the density-matrix-renormalization-group (DMRG) approaches. Consequently, our results are qualitatively consistent with all the above experiments: The enhanced T_c with enhanced Nd-substitution fraction, the dome shaped T_c with enhanced pressure, and the enhanced

T_c with compressive strain are all determined by the corresponding variation of J_{\perp} with experimental conditions; the suppression of T_c by hole doping is caused by reduction of the filling fraction. As a comparison, we also adopt the weak-coupling RPA approach to study these experiments. Consequently, except the pressure-dependence of T_c , none of the above experiments can be well understood by RPA. Our results not only help to clarify the pairing mechanism in $\text{La}_3\text{Ni}_2\text{O}_7$, but also provide guidance to enhance its T_c : We propose that electron doping realized through substitution of La^{3+} by element with higher valence, either in pressurized bulk or in compressive-strained film, or further enhancement of the compressive strain in the film can enhance T_c .

II. MODEL, APPROACHES AND ITS PROPERTIES

$\text{La}_3\text{Ni}_2\text{O}_7$ hosts a quasi-two-dimensional bilayer structure, in which the nearly half-filled Ni - $3d_{z^2}$ orbital and the nearly quarter-filled $3d_{x^2-y^2}$ orbital dominate the low-energy degrees of freedom. The d_{z^2} -orbitals acquire an interlayer hopping t_{\perp}^z through hybridization with the apical-oxygen p_z orbitals, while the $d_{x^2-y^2}$ orbitals form an intralayer hopping t_{\parallel}^x through hybridization with the in-plane O- $p_{x(y)}$ orbitals. The strong Hubbard repulsion U between Ni-3d electrons leads to a strong interlayer antiferromagnetic (AFM) superexchange J_{\perp}^z between the d_{z^2} -orbitals and a relative weaker intralayer AFM superexchange J_{\parallel}^x between the $d_{x^2-y^2}$ -orbitals. Plus the Hund's coupling J_H , the schematic diagram is shown in Fig. 1 (a).

In the strong-coupling picture, the nearly half-filled d_{z^2} orbital is almost localized. Note that there exists considerable intralayer nearest-neighbor (NN) hybridization between the two $3d E_g$ orbitals in the DFT level, which enhances the mobility of the d_{z^2} orbital electrons. However, such hybridization itself will be strongly suppressed by the strong electron correlation because the achievement of the hybridization requires the motion of the nearly half-filled d_{z^2} -orbital electrons, which is strongly blocked by the strong Hubbard repulsion U . Therefore, we ignore such interorbital hybridization and hold the viewpoint that the nearly-quarter-filled $d_{x^2-y^2}$ orbital electrons dominantly carry SC in the system.

The interlayer AFM superexchange interaction J_{\perp}^z leads to strong interlayer AFM correlation between d_{z^2} -orbital electrons. Then the strong Hund's coupling transfers such interlayer AFM correlation to the $d_{x^2-y^2}$ electrons, leading to an effective interlayer superexchange interaction J_{\perp} between the $d_{x^2-y^2}$ electrons. Consequently, we obtain the following effective $d_{x^2-y^2}$ -orbital bilayer $t - J_{\parallel} - J_{\perp}$ model proposed previously in Refs. [37, 38, 49, 55, 56, 59, 69, 110–112, 115–117, 120, 121],

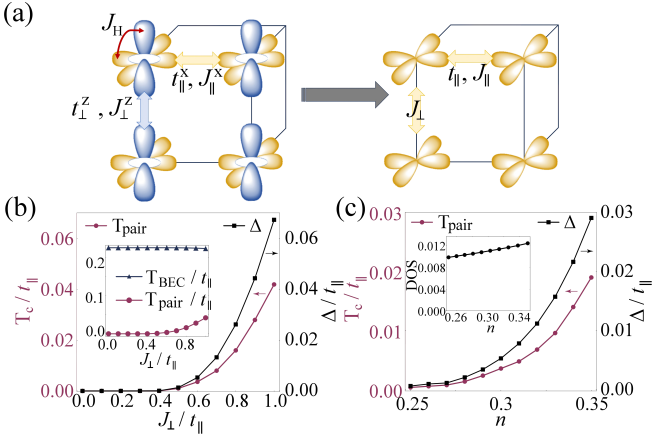


FIG. 1. Schematic diagram and properties of the models. (a) Schematic diagram of the two-orbital $t - J - J_H$ model (left) and the one-orbital $t - J_\parallel - J_\perp$ model (right). (b) The relationship between T_c (red line) and SC gap Δ (blue line) of the $t - J_\parallel - J_\perp$ model and the interlayer superexchange parameter J_\perp . The inset compares between the BEC temperature T_{BEC} and pairing temperature T_{pair} , and the results show that T_c is determined by T_{pair} . (c) The relationship between T_c (red line) and SC gap Δ (blue line) of the $t - J_\parallel - J_\perp$ model and the filling fraction n . The inset shows the relationship between DOS and the filling fraction. In (b) and (c), the left and right arrows point to the y -axis correspond to the two lines.

$$H = - \sum_{i,j,\alpha,\sigma} \mathcal{P} t_{ij} (c_{i\alpha\sigma}^\dagger c_{j\alpha\sigma} + \text{h.c.}) \mathcal{P} + J_\parallel \sum_{\langle i,j \rangle, \alpha} \mathbf{S}_{i\alpha} \cdot \mathbf{S}_{j\alpha} + J_\perp \sum_i \mathbf{S}_{i1} \cdot \mathbf{S}_{i2}. \quad (1)$$

Here, $c_{i\alpha\sigma}^\dagger$ ($c_{i\alpha\sigma}$) is the creation (annihilation) operator of the $d_{x^2-y^2}$ electron at the i site in the α -th layer ($\alpha = 1, 2$) with spin σ . The t_{ij} is the hopping of the $d_{x^2-y^2}$ orbital, and the main hopping is the intralayer NN hopping t_\parallel . \mathcal{P} is the Gutzwiller projector to exclude double occupancy at the same site. $\mathbf{S}_{i\alpha}$ is spin operator of the $d_{x^2-y^2}$ orbital at the i site in the α -th layer, and $\langle i, j \rangle$ represents intralayer NN sites.

The strength J_\perp of the effective interlayer superexchange interaction between the $d_{x^2-y^2}$ orbitals appearing in Eq. (1) can be estimated through a comparative DMRG study. Using DMRG, we calculate the interlayer spin correlations between the $d_{x^2-y^2}$ orbitals $\langle \mathbf{S}_{i1}^x \cdot \mathbf{S}_{i2}^x \rangle$ for two different models: one is the two-orbital $t - J - J_H$ model shown in the left panel of Fig. 1(a) and the other is the single $d_{x^2-y^2}$ -orbital bilayer $t - J_\parallel - J_\perp$ model shown in the right panel of Fig. 1(a) represented by Eq. (1). Adjusting J_\perp so that the obtained $\langle \mathbf{S}_{i1}^x \cdot \mathbf{S}_{i2}^x \rangle$ for the two models are equal, the J_\perp thus obtained is the resultant strength of the effective superexchange. It is interesting to note that $J_\perp > J_\perp^z$ is possible, particularly for weak J_\perp^z/J_H , which is different from the previous understanding [121], because of the following

reason. In the two-orbital model, due to the localized nature of the d_{z^2} orbitals, a weak J_\perp^z is enough to generate considerable AFM correlation $\langle \mathbf{S}_{i1}^z \cdot \mathbf{S}_{i2}^z \rangle$, which is transferred to the $d_{x^2-y^2}$ orbitals to generate considerable $\langle \mathbf{S}_{i1}^x \cdot \mathbf{S}_{i2}^x \rangle$ through the strong Hund's rule. In the single $d_{x^2-y^2}$ -orbital model, to generate the equivalent value of $\langle \mathbf{S}_{i1}^x \cdot \mathbf{S}_{i2}^x \rangle$, a stronger J_\perp might be required due to the itinerant nature of the $d_{x^2-y^2}$ orbital electrons, because the large FS of the $d_{x^2-y^2}$ electrons are robust against the formation of AFM correlation $\langle \mathbf{S}_{i1}^x \cdot \mathbf{S}_{i2}^x \rangle$ under weak J_\perp . This reason makes $J_\perp > J_\perp^z$ possible for weak J_\perp^z . See more details in Appendix A.

Then we introduce the properties of the $t - J_\parallel - J_\perp$ model. Previous studies have shown robust interlayer s-wave SC under the parameters corresponding to the realistic materials in this model. We thus set the intralayer AFM superexchange $J_\parallel = 0$ in this work because it does not obviously influence the interlayer pairing. We shall employ the SBMF theory [122, 123] and DMRG method [124] to study this model as strong coupling approaches in the following.

In the SBMF theory, the electron operator $c_{i\alpha\sigma}^\dagger$ can be decomposed as $c_{i\alpha\sigma}^\dagger = f_{i\alpha\sigma}^\dagger b_{i\alpha}$, wherein the fermionic spinon $f_{i\alpha\sigma}^\dagger$ and the bosonic holon $b_{i\alpha}$ satisfy the no-double-occupancy constraint $\sum_\sigma f_{i\alpha\sigma}^\dagger f_{i\alpha\sigma} + b_{i\alpha}^\dagger b_{i\alpha} = 1$. The onset of SC requires that the spinons pair and the holons are Bose-Einstein condensed (BEC) simultaneously. Therefore, we have $T_c = \min\{T_{\text{pair}}, T_{\text{BEC}}\}$, where T_{pair} represents for the onset temperature for the spinons to pair and T_{BEC} indicates the BEC temperature of the holons. In the SBMF, we define the following order parameters:

$$\begin{aligned} \chi_{\parallel\alpha}^* &= \langle f_{i\alpha\uparrow}^\dagger f_{j\alpha\uparrow} + f_{i\alpha\downarrow}^\dagger f_{j\alpha\downarrow} \rangle, \\ \chi_{\perp}^* &= \langle f_{i1\uparrow}^\dagger f_{i2\uparrow} + f_{i1\downarrow}^\dagger f_{i2\downarrow} \rangle, \\ \Delta^* &= \langle f_{i1\uparrow}^\dagger f_{i2\downarrow}^\dagger - f_{i1\downarrow}^\dagger f_{i2\uparrow}^\dagger \rangle. \end{aligned} \quad (2)$$

which describe the intralayer and interlayer bonding and interlayer pairing. T_{pair} is decided by the temperature when $\Delta \rightarrow 0$ through solving the self-consistent gap equation, and T_{BEC} is calculated by the Kosterlitz-Thouless (KT) transition:

$$T_{\text{BEC}} = T_{\text{KT}} = \frac{\pi}{2} \tilde{\rho} = \frac{\pi}{2} \tilde{t}_{\parallel\alpha} \delta \quad (3)$$

in which $\tilde{\rho}$ is the superfluid density, $\tilde{t}_{\parallel\alpha}$ is the renormalized intralayer hopping $\tilde{t}_{\parallel\alpha} = t_\parallel \chi_{\parallel\alpha}$, and δ is the density of the holon. See more details of the SBMF theory in Appendix B. In bilayer nickelates $\text{La}_3\text{Ni}_2\text{O}_7$, as the $d_{x^2-y^2}$ -orbital electrons are nearly quarter-filled, the large $\delta \approx 0.5$ and large t_\parallel lead to large $T_{\text{BEC}} \gg T_{\text{pair}}$, as shown in the insets of Fig. 1 (b). Therefore, we have $T_c = T_{\text{pair}}$, similar with the overdoped cuprates.

Fixing the filling fraction $n = 0.3$ that is close to realistic bulk materials, we change J_\perp to study how it affects SC, with the results shown in Fig. 1 (b). The inset of

Fig. 1 (b) shows that T_{BEC} almost does not change with J_{\perp} due to the fixed filling fraction, and is much larger than T_{pair} for realistic J_{\perp} , ensuring $T_c = T_{\text{pair}}$. The main panel of Fig. 1 (b) shows T_c and the ground state pairing strength Δ in unit of t_{\parallel} as function of J_{\perp}/t_{\parallel} . Obviously, we find $T_c \propto \Delta$ and both increase promptly with the enhancement of J_{\perp} , which is within expectation.

Then, fixing $J_{\perp} = 0.6t_{\parallel}$ as a typical parameter, we study the filling fraction n -dependence of the SC, with the results shown in Fig. 1 (c). The inset of Fig. 1 (c) shows that T_{BEC} starts with a large number, then decreases gradually with filling fraction. In the whole range of realistic n , we have $T_{\text{BEC}} \gg T_{\text{pair}}$, setting $T_c = T_{\text{pair}}$. The main panel of Fig. 1 (c) shows the n -dependence of T_c and Δ , suggesting $T_c \propto \Delta$ and both increase with the enhancement of n . This result can be understood in the framework of the Bardeen-Cooper-Schrieffer (BCS) theory, which states

$$T_c \propto \Delta \sim e^{-1/(N_{E_f} J_{\perp})}, \quad (4)$$

where N_{E_f} indicates the DOS near the FS. In this model, the increase of the filling fraction n leads to an increase of N_{E_f} , resulting in a significant increase in T_c and Δ .

To capture the quantum fluctuation effect beyond the SBMF, we also employ DMRG method to study the $t - J_{\parallel} - J_{\perp}$ model. Tensor libraries TensorKit [125] and FiniteMPS [126] provide an implementation of the required symmetry [127, 128]. We keep up to $D = 6400$ $U(1)_{\text{charge}} \times SU(2)_{\text{spin}}$ multiplets to study the model on a $2 \times 1 \times 128$ ladder and ensure the convergence accuracy of 10^{-8} . In DMRG calculations, we mainly calculate the interlayer pairing correlation function $\Phi^{\perp}(r) = \langle \Delta_i^{\perp \dagger} \Delta_j^{\perp} \rangle$ to characterize SC in the ground state, in which the interlayer pairing operator $\Delta_i^{\perp \dagger}$ is defined as $\Delta_i^{\perp \dagger} = \frac{1}{\sqrt{2}} (c_{i1\uparrow}^{\dagger} c_{i2\downarrow}^{\dagger} - c_{i1\downarrow}^{\dagger} c_{i2\uparrow}^{\dagger})$. In the 1D system where DMRG works, the pairing correlation typically decays algebraically as $r^{-K_{\text{SC}}}$, leading to a quasi-long-range order. The decay power exponent K_{SC} is related to the Luttinger parameter, which is negatively correlated with SC.

In the following sections, we focus on how changes in experimental conditions affect the two key parameters, J_{\perp} and n , which result in variations in T_c and Δ . In this work, we adopt the hopping parameters from previous DFT calculations, and adopt J_{\perp}^z from the DFT results or simply from $J_{\perp}^z = 4(t_{\perp}^z)^2/U$ with $U \approx 5$ eV in some cases. Based on previous studies [45, 49, 61, 64, 129, 130], we adopt $J_H = 1$ eV. We have also tried weaker $J_H = 0.8$ eV and 0.6 eV, which lead to similar results.

III. EFFECT OF J_{\perp} ON T_c

In this section, we study how T_c evolves with experimental conditions which mainly tune the strength of J_{\perp} . These experiments include the rare-earth Nd/Sm-

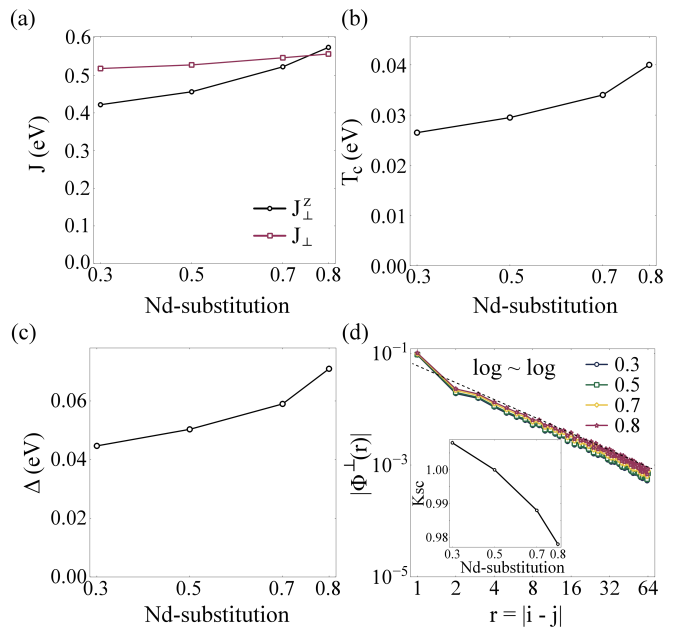


FIG. 2. Mechanism and results on Nd substitution in bulk. (a) The interlayer superexchange parameters $J_{\perp}^z = 4t_{\perp}^z{}^2/U$ (black line) and J_{\perp} (red line) change with Nd substitution, where $U = 5$ eV. (b) The T_c as a function of Nd substitution calculated by SBMF theory. (c) The SC gap as a function of Nd substitution calculated by SBMF theory. (d) The interlayer pairing correlation function $|\Phi^{\perp}(r)|$ calculated by DMRG. The decay power exponents K_{SC} are plotted in the inset as a function of Nd substitution. The legend “log ~ log” corresponds to a log-log plot. The line legends in the figures indicate their meanings.

element substitutions, the variation of pressure, the tuning of compressive strain, which will be studied separately in the following subsections.

A. Nd/Sm Substitution in pressurized Bulk $\text{La}_3\text{Ni}_2\text{O}_7$

The substitution of La by rare-earth elements such as Nd or Sm in $\text{La}_3\text{Ni}_2\text{O}_7$ has been found to play an important role in enhancing T_c . Recently, the partial substitution of La by Sm to form $\text{La}_2\text{SmNi}_2\text{O}_7$ and $\text{La}_{1.57}\text{Sm}_{1.43}\text{Ni}_2\text{O}_{7-\delta}$ has enhanced the T_c to 92 K and 96 K respectively [96]. Another Sm-substitution to form $\text{La}_{3-x}\text{Sm}_x\text{Ni}_2\text{O}_7$ also improves T_c to 89 K by different growth methods [98]. Similarly the partial substitution of La by Nd to form $\text{La}_{3-x}\text{Nd}_x\text{Ni}_2\text{O}_7$ shows that $T_c \sim 93$ K for $x = 2.1$ and 2.4 in electronic transport measurement, and $T_c \sim 98$ K for $x = 2.4$ tested by radio-frequency transmission technique [97]. In addition, T_c shows a trend of increasing with the fraction of Nd-substitution [97].

Physically, the rare-earth elements substitution enhances T_c through the tuning of J_{\perp} , as previously predicted in Ref. [56] ahead of the experiments. Structurally,

through substitution of La by rare-earth elements Ce, Pr, Nd, Pm and Sm, the lattice constant under the pressure corresponding to the structure transition gradually shrinks, because of the gradually reduced radius of the rare-earth atoms. A direct consequence of such element substitution is the gradual increase of the hopping integrals t_{ij} . Then, through the relation $J \propto t^2/U$, the superexchange J_{\perp} increases even stronger than t_{ij} , resulting in enhanced J_{\perp}/t_{\parallel} , which enhances T_c . While the study conducted in Ref. [56] is focused on the effect of full element substitution, the effect of partial element substitution relevant to experiments will be studied here.

In this subsection, we use the tight-binding (TB) model fitted for varying Nd-substitution fraction x provided in Ref. [131] to study how T_c changes with x . We use $J_{\perp}^z = 4(t_{\perp}^z)^2/U$ and adopt $U = 5$ eV to estimate the interlayer AFM superexchange interaction between the d_{z^2} orbitals J_{\perp}^z . The resulting $J_{\perp}^z \sim x$ shown in Fig. 2 is similar with that obtained through exact diagonalization of a small cluster conducted in Ref. [131]. Then we use the DMRG methods introduced in Sec. II to estimate the effective J_{\perp} in our $t - J_{\parallel} - J_{\perp}$ model Eq. (1). Similar to the case of full element substitution, Fig. 2 (a) shows that both J_{\perp}^z and J_{\perp} increase with the enhancement of Nd-substitution fraction x .

Then we use SBMF theory to calculate the T_c and the ground-state gap amplitude Δ as functions of the Nd-substitution fraction x . As shown in Fig. 2 (b) and (c), both T_c and Δ increase with Nd-substitution, which is caused by the increasing interlayer superexchange J_{\perp} as explained in Sec. II. Although the filling fraction n slightly increases with Nd-substitution as mentioned in Ref. [131], it is not the main cause of the increase in T_c .

Fig. 2 (d) shows the DMRG results that the interlayer pairing correlation functions $|\Phi^{\perp}(r)|$ decay algebraically, implying the presence of pairing between layers in realistic 2D system. With an increase in the Nd-substitution level, the pairing correlation strength increases, manifested as a higher value of the correlation function $|\Phi^{\perp}(r)|$ at the same distance r . Additionally, the decay power exponent K_{SC} decays with Nd-substitution as shown in the inset, which means a slower decay of $|\Phi^{\perp}(r)|$ and suggests an enhancement of SC in the 2D system. The combined results indicate that Nd-substitution improves SC, which is consistent with our SBMF results. More DMRG results are detailed in **Appendix C**.

Our results are qualitatively consistent with the experiment [97], which reveals that c-axis lattice constants for Nd-substitution fraction $x = 2.1 - 2.4$ is comparable with those for Sm-substitution fraction $x = 1.5$ and both have an approximate T_c . Our results also support the conclusion [97] that T_c is inversely proportional to the c-axis lattice constant, implying that shorter c-axis lattice constant leads to stronger interlayer hopping, and consequently leads to strengthened interlayer AFM superexchange and hence enhanced SC.

B. Pressure-Dependence in the Bulk

In bulk $\text{La}_3\text{Ni}_2\text{O}_7$, SC arises at the pressure $P \sim 14$ GPa with a structural transition, and T_c reaches the maximum of 83 K at $P \sim 18$ GPa, then gradually decreases with pressure and vanishes above $P \sim 80$ GPa, forming a right-triangle-like SC region [8]. Several theoretical studies investigate this phenomenon and attribute it to FS nesting [62], spin fluctuations [81], or a change in the ratio of interaction to hopping integral and favor of competitive phase [132]. Here we study the problem through our $t - J_{\parallel} - J_{\perp}$ model Eq. (1).

We adopt the TB parameters provided in Ref. [133]. This literature also provides the DFT result for the interlayer superexchange interaction between the d_{z^2} orbitals J_{\perp}^z , calculated by the energy difference between the ferromagnetic (FM) and the A-type AFM configurations [133, 134], with the result shown in Fig. 3(a). With increased pressure, the obtained value of J_{\perp}^z first arises promptly until $P \sim 30$ GPa where it reaches its maximum, and then gradually decreases until $P \sim 80$ GPa, where its value is close to that at ambient pressure. Such a dome shaped $J_{\perp}^z \sim P$ relation mimics the $T_c \sim P$ relation observed experimentally. The physical reason for such dome shaped $J_{\perp}^z \sim P$ relation is as following. In the low- P regime, with the enhancement of P , the interlayer Ni-O-Ni bonding angle promptly saturates to 180° , leading to enhanced interlayer hopping and hence enhanced J_{\perp}^z through the superexchange mechanism. It is important to note that an additional effect of pressure is to raise the energy level of O- p_z orbital, to make it cross the Fermi level and to bring influence on the superexchange mechanism. This effect leads to the decrease of J_{\perp}^z above the pressure $P \sim 30$ GPa, and finally forms the dome shaped $J_{\perp}^z \sim P$ relation. Due to change of the superexchange mechanism, the relation $J_{\perp}^z = 4(t_{\perp}^z)^2/U$ no longer stands for large P , and therefore we adopt the DFT value of J_{\perp}^z provided in Ref. [133] as our input for subsequent studies.

We calculate the effective J_{\perp} for our $t - J_{\parallel} - J_{\perp}$ model according to the method introduced in Sec. II using DMRG. As shown in Fig. 3 (a), the trend of J_{\perp} with P is the same as that of J_{\perp}^z , but it is more gradual. J_{\perp} reaches its maximum at 30 GPa and then slowly drops. We calculate T_c and Δ using the SBMF theory, which both suddenly increase accompanying the structural transition at 10-20 GPa, reach their maximum values at 30 GPa, and then gradually decrease, as shown in Fig. 3 (b) and (c). The values of T_c and Δ at 80 GPa are close to that of 10 GPa, implying that SC is completely suppressed under such high pressure. Although the filling fraction slightly increases with pressure according to the DFT calculation [133], T_c and Δ still decrease above 30 GPa, caused by the decrease in J_{\perp} .

The interlayer pairing correlation functions $|\Phi^{\perp}(r)|$ calculated by DMRG are shown in Fig. 3 (d). The correlation strength first increases and then decreases with increasing pressure, consistent with the dome-like trend

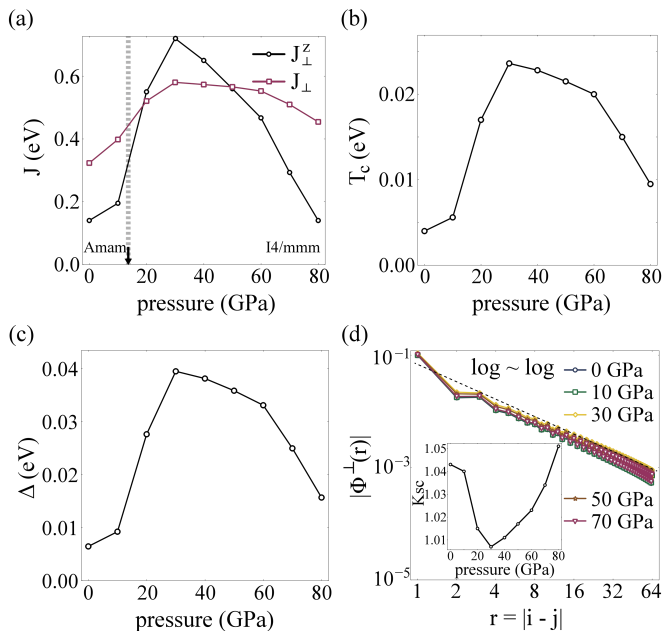


FIG. 3. Mechanism and results on pressure-dependence in bulk. (a) The interlayer superexchange parameters J_{\perp}^z (black line) from DFT and J_{\perp} (red line) calculated by DMRG change with pressure. The gray dash line and black arrow label the structural transition. (b) The T_c as a function of pressure calculated by SBMF theory. (c) The SC gap as a function of pressure calculated by SBMF theory. (d) The interlayer pairing correlation function $|\Phi^+(r)|$ calculated by DMRG.

of J_{\perp} . In contrast, the decay power K_{SC} exhibits an opposite behavior of first decreasing and then increasing. These combined results imply a pressure-dependent dome-like SC phase, consistent with our SBMF results.

Both our SBMF results and the DMRG calculation show a similar behavior to the experiments [8] that SC arise with pressure at 10-20GPa, T_c reaches the maximum near 20GPa, then gradually decreases until SC is completely suppressed at ~ 80 GPa.

C. Strain-Dependence in the Film

The experiment finds that $\text{La}_3\text{Ni}_2\text{O}_7$ thin films which are grown on SrLaAlO_4 substrates that lead to about -2% compressive strain, exhibits SC with $T_c \sim 42$ K at ambient pressure, but thin films with no substrate or tensile substrate have no SC [82]. SC is also found in $(\text{La},\text{Pr})_3\text{Ni}_2\text{O}_7$ film [83] and $\text{La}_2\text{PrNi}_2\text{O}_7$ film [84] with $T_c=40\sim 50$ K on SrLaAlO_4 substrate. Using improved technology, the thin film $\text{La}_2\text{PrNi}_2\text{O}_7$ on LaAlO_3 substrates which compress the film $\sim 1.2\%$ is with T_c decreased to ~ 10 K [135]. These experiments imply that the turning compression strain is a key factor in T_c . Some studies understand SC in $\text{La}_3\text{Ni}_2\text{O}_7$ (SrLaAlO_4) from a weak coupling perspective [104, 106–109, 136–139]. Here we use SBMF and DMRG to study the $t - J_{\parallel} - J_{\perp}$ model as the strong

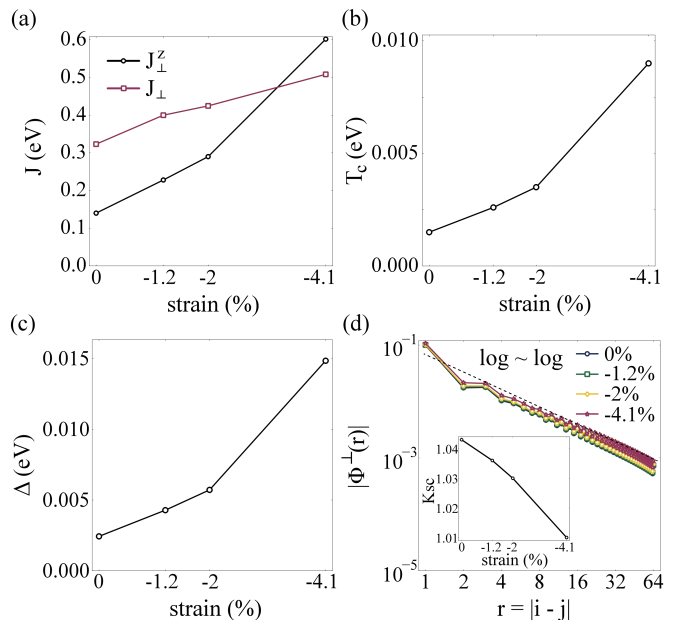


FIG. 4. Mechanism and results on strain-dependence in the film. (a) The interlayer superexchange parameters J_{\perp}^z (black line) from DFT and J_{\perp} (red line) calculated by DMRG change with strain. (b) The T_c as a function of strain calculated by SBMF theory. (c) The SC gap as a function of strain calculated by SBMF theory. (d) The interlayer pairing correlation function $|\Phi^+(r)|$ calculated by DMRG.

coupling approach.

In this subsection, we adopt the TB parameters and J_{\perp}^z in Ref. [133] in which J_{\perp}^z is obtained by DFT through calculating the energy difference between the FM and the A-type AFM configurations [133, 134]. As shown in Fig. 4(a), J_{\perp}^z increases with compressive strain. The physical origin for this lies in that, with compressive strain, the apical Ni-O-Ni bonding angle gradually increases to 180° [85, 86, 109, 138, 140, 141], which leads to enhanced interlayer hopping t_{\perp}^z [106, 109, 133, 140] and hence enhanced interlayer AFM superexchange J_{\perp}^z .

We calculate the effective J_{\perp} using the method introduced in Sec. II by DMRG. As shown in Fig. 4(a), when compressive strain enhances, following the increase of J_{\perp}^z , our calculated effective J_{\perp} also increases, but more gently. Then we calculate T_c and Δ using SBMF theory, which are shown in Fig. 4 (b) and (c). They both increase with compressive strain, which is caused by increased J_{\perp} .

Fig. 4 (d) shows the algebraic decay of $|\Phi^+(r)|$ calculated by DMRG. The pairing correlation strength increases with compressive strain. In contrast, the decay power exponent K_{SC} decays as shown in the inset. These combined results imply an enhancement of SC with compressive strain, consistent with the SBMF results.

Our results show that as compressive strain increases, SC is improved by increasing interlayer AFM superexchange J_{\perp}^z . These results are qualitatively consistent with the experiments [82, 135], and give suggestion to the strain-tuning for SC that T_c could be enhanced by

further strengthening the compressive strain.

IV. EFFECT OF HOLE-DOPING ON T_c

Besides changing the factors which influence J_{\perp} , another control method for the nickelates is to change the charge carrier concentration. Two approaches are available for this purpose: one is to tune the oxygen content, and the other is heterovalent element substitution. In this section, we study how the change of charge carrier, specifically hole doping, influences T_c , and compare with the following relevant experiments.

Let us first focus on the experiments that tune oxygen content. Recently, the T_c of the thin film of $(\text{La,Pr})_3\text{Ni}_2\text{O}_7$ grown on top of the SrLaAlO_4 substrate reaches ~ 63 K by improved experimental methods [118], which makes further progress on the nickelate SC at ambient pressure. In this experiment, T_c is maximized at the optimal oxidization, which might probably corresponds to the situation in which most oxygen vacancies have been eliminated. Upon further oxidization, the overdoped oxygen atoms enter interstitial sites between NiO_2 layers [119], which lowers the T_c . This phenomenon is similar to the experiment in bulk $\text{La}_2\text{PrNi}_2\text{O}_{7+\delta}$ under high pressure that overdoped oxygen atoms also enter interstitial sites and suppress SC [142]. Since these interstitial oxygen atoms are far from the NiO_2 layers, the possible direct influence of them on the electronic structure within the NiO_2 layers is to generate excess holes. These experiments suggest that hole doping induced through over-oxidization, either in the pressurized bulk material or in the strained film at ambient pressure, suppresses SC.

Let us then study the experiment on heterovalent element substitution. In this aspect, the alkaline earth element Sr^{2+} -doping into the $\text{La}_3\text{Ni}_2\text{O}_7$ thin films to form $\text{La}_{3-x}\text{Sr}_x\text{Ni}_2\text{O}_7$ has been conducted in Ref. [90]. Here x indicates the Sr-doping fraction, which is related to the hole doping level δ via the relation $\delta = x/2$. In this experiment, it is found that with the enhancement of x , the T_c first increases slightly in the regime $x \in (0, 0.1)$ and then slowly decreases in the regime $x \in (0.1, 0.38)$, and SC vanishes at $x > 0.38$. At first glance, it seems that the hole doping dependence of T_c here for the Sr^{2+} -doping is slightly different from that for the over-oxidization introduced above. However, it should be aware that the effect of Sr^{2+} -doping in $\text{La}_{3-x}\text{Sr}_x\text{Ni}_2\text{O}_7$ is not simply to induce holes: it additionally enhances the interlayer AFM superexchange interaction J_{\perp}^z and hence J_{\perp} through shortening the c -axis lattice constant. Actually, it is reported in Ref. [90] that with the enhancement of x , the c -axis lattice constant first abruptly decreases in regime $x \in (0, 0.1)$ and then slowly decreases in regime $x > 0.1$. Therefore, if the additional compensatory effect, i.e. increasing the interlayer AFM superexchange interaction, was removed, the remaining net effect, i.e. hole doping, caused by Sr^{2+} -doping should obviously suppress

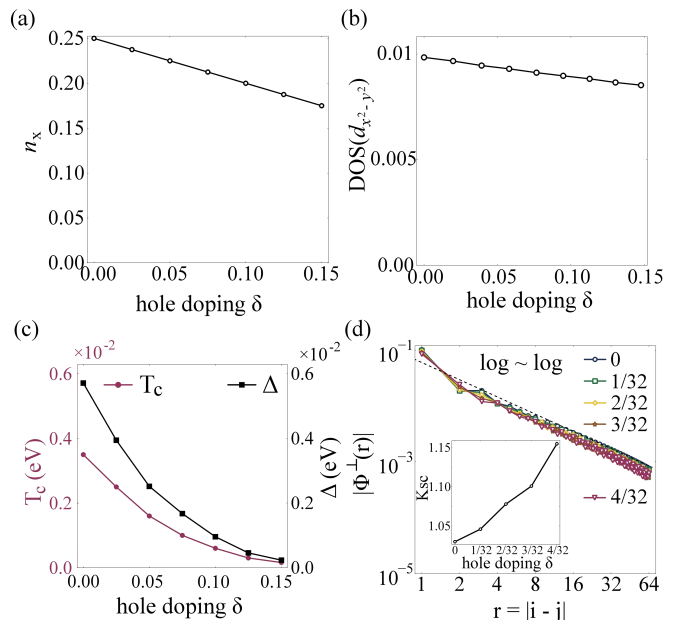


FIG. 5. Mechanism and results on hole doping in the film. (a) The filling fraction of $d_{x^2-y^2}$ -orbital electrons changes with hole doping. (b) The DOS of $d_{x^2-y^2}$ -orbital as a function of hole doping. (c) The T_c and SC gap as functions of hole doping calculated by SBMF theory. (d) The interlayer pairing correlation functions $|\Phi_{\perp}^{\pm}(r)|$ with different hole doping level δ calculated by DMRG.

SC, similar to the case in the over-oxidization. Note that recent experiment with Ca^{2+} -doping into the film [119] also arrives at the conclusion that hole-doping caused by alkaline earth element substitution suppresses SC.

The suppression of SC by hole doping revealed in the above introduced experiments can be well understood in our $t - J_{\parallel} - J_{\perp}$ model. Here we consider the $\text{La}_3\text{Ni}_2\text{O}_7$ thin film grown on top of the SrLaAlO_4 substrate with $\sim 2\%$ compressive strain, and adopt the TB parameters and the DFT J_{\perp}^z from Ref. [133]. To obtain the filling fraction of the $d_{x^2-y^2}$ orbital n_x in our single-orbital $t - J_{\parallel} - J_{\perp}$ model, we start from the full two-orbital TB model and adjust the chemical potential to simulate hole doping, from which we calculate n_x . As informed by the DFT calculations, the γ pocket of d_{z^2} orbital is below the Fermi level, and so the DOS is mainly contributed by the $d_{x^2-y^2}$ orbital. Therefore, doped holes enter mainly into the $d_{x^2-y^2}$ orbitals until the γ pocket crosses the FS. The filling fraction of the $d_{x^2-y^2}$ orbital n_x decreases with hole doping level $\delta = x/2$, as shown in Fig. 5 (a). The decrease in n_x leads to the decrease of DOS, as displayed in the inset of Fig. 5 (b). Due to decrease of the DOS, our SBMF calculations reveal that T_c and Δ decrease with hole doping, as shown in Fig. 5 (c).

Our DMRG results shown in Fig. 5 (d) exhibits a similar physical picture. Hole-doping reduces carriers, leading to weaker pairing correlation strength. However, due to size effects, the system is relatively sensitive to changes in particle number, so this point does not hold universally

for all distances r . On the contrary, the decay exponent K_{SC} shows a more robust trend, which is positively related to the hole doping level, suggesting a weakening of SC, consistent with the SBMF results.

Our results are consistent with the experiments of alkaline earth element substitution and over-oxidization in the thin films, that T_c is suppressed by hole doping. Note that hole doping in the pressurized bulk material is slightly different in that the doped holes can enter both the $d_{x^2-y^2}$ and d_{z^2} orbitals which both have DOS near the FS. The hole doping of d_{z^2} orbital reduces its occupation number, and hence reduces the probability of transferring the interlayer superexchange interaction from d_{z^2} orbital to $d_{x^2-y^2}$ orbital, leading to reduced J_{\perp} ; and the hole doping of $d_{x^2-y^2}$ orbital decreases its filling fraction n_x . Since both reduced J_{\perp} and reduced n_x suppress SC, our model yields that hole doping suppresses SC in the pressurized bulk material as well, which is consistent with experiment [142].

While the hole doping suppresses T_c , the electron doping would, on the contrary, enhance T_c : Upon electron doping, the filling fraction of the $d_{x^2-y^2}$ orbitals n_x would be enhanced. As shown in the inset of Fig. 1(c), following the enhancement of n_x , the DOS of the $d_{x^2-y^2}$ orbital would be enhanced. Then Eq. (4) suggests that the T_c would increase promptly. Two approaches are possible to realize electron doping in $\text{La}_3\text{Ni}_2\text{O}_7$: (1) to decrease oxygen content and (2) to substitute La with elements with valence higher than +3. While the first approach would suffer from the notorious problem of oxygen vacancy [1, 9, 119, 142, 143], which strongly suppresses SC, we are left with the second one. Then we predict here that the implement of electron doping through substitution of La by element with valence higher than +3 would obviously enhance T_c , either in the film under compressive strain or in the bulk under pressure.

V. IN COMPARISON WITH RPA RESULTS

As a comparison with our strong-coupling studies, we perform the RPA-based calculation to investigate the experimental controlling of the T_c of bilayer nickelates within the itinerant electron picture, and compare our RPA results with some present weak-coupling studies. Starting from TB model, which is equipped with the standard multiorbital Hubbard interaction, RPA-based calculation studies the SC mediated by short-range spin fluctuations. The SC critical temperature T_c can be estimated by the pairing eigenvalue λ as $T_c \sim e^{-1/\lambda}$.

Specifically, we calculate the effects of Nd-substitution, pressure, compressive strain, and hole doping on SC in bilayer nickelates, with the results illustrated by the red lines in Fig. 6. In pressured bulk $\text{La}_3\text{Ni}_2\text{O}_7$, as the Nd-substitution level increases, the λ decreases as indicated by the red line in Fig. 6(a), suggesting that Nd-substitution suppresses SC, which is contrary to the experimental results [97]. Fig. 6(b) presents the pressure

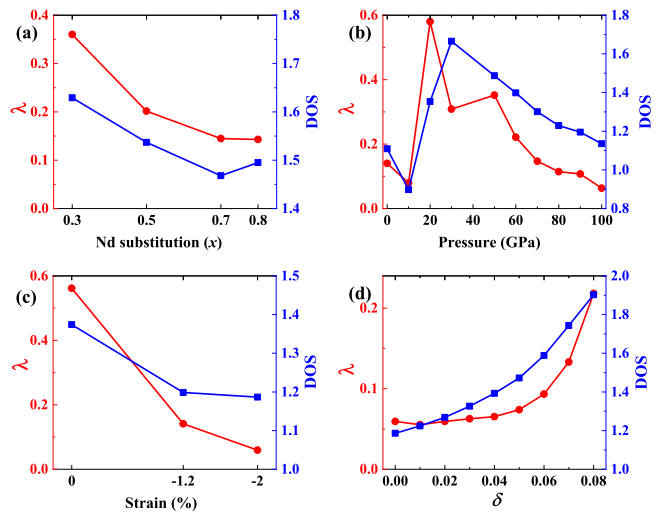


FIG. 6. The pairing eigenvalue λ (red line) calculated by RPA and DOS (blue line) as the function of (a) Nd-substitution level x in $\text{La}_{3-x}\text{Nd}_x\text{Ni}_2\text{O}_7$ bulk materials; (b) the pressure in $\text{La}_3\text{Ni}_2\text{O}_7$ bulk materials; (c) the strain in $\text{La}_3\text{Ni}_2\text{O}_7$ thin film; (d) hole doping level δ in $\text{La}_3\text{Ni}_2\text{O}_7/\text{SrLaAlO}_4$ thin film. The electron number fixes $n = 1.5$ for RPA calculation except (d). We adopt $U = 1.2$ eV in (a,c,d), and $U = 1.1$ eV in (b).

dependence of SC. Upon the application of pressure, λ rises sharply until the pressure reaches 20 GPa, and more pressure suppresses SC. This trend is qualitatively consistent with experimental observations [8]. For the SC in $\text{La}_3\text{Ni}_2\text{O}_7$ thin film, as shown in Fig. 6(c), with increasing compressive strain, λ decreases, indicating that the compressive strain provided by the substrate prevents SC. This result, however, contradicts the experimental results. Furthermore, either the Sr-substitution or excess oxygen content suppresses SC by inducing hole doping in thin films [90, 118]. The corresponding RPA calculations are shown in Fig. 6(d), in which λ continues to increase with increasing hole doping, suggesting that hole doping enhances SC, which is in contrast with experimental findings [90, 118]. In conclusion, except the pressure-dependence of T_c , none of the above experiments can be well understood by our RPA results.

To understand our RPA results, we also provide the corresponding DOS for each case, as shown by the blue lines in all panels of Fig. 6. It is evident that λ and DOS in all panels exhibit the same variation trend, which implies that within the itinerant electron picture, the DOS of the system plays a crucial role in SC, which is also supported by other weak-coupling studies on nickelate SC [103, 105, 106]. Therefore, in order to provide a unified understanding of all the calculation results, we reproduce all the DOS curves from Fig. 6 and plot them together in Fig. 7(a). In Fig. 7(a), the DOS curves under variations in Nd-substitution, pressure, compressive strain, and hole doping are represented by the black, red, blue, and green lines, respectively, and the corresponding horizontal coordinates adopt the same color as the DOS

curves. Furthermore, from left to right, Fig. 7(a) is divided into four regions, marked by Roman numerals I~IV, and separated by gray dashed lines. In each region, the FS and band structure near Fermi energy of the systems corresponding to the parameter points in this region are qualitatively illustrated in Fig. 7(b,c) below.

Next, we present a detailed introduction to the evolution of the FS and band structure from the left to the right of Fig. 7(a) (i.e., from region I to region IV), which is helpful to understand the variation in the DOS. In region I, the far left of Fig. 7(a), only α and β pockets exist, and the d_{z^2} -orbital bonding band lies entirely below the Fermi energy, as shown in Fig. 7(b,c) below region I. Experimentally, when the compressive strain in the thin film decreases from -2% to 0, or when the thin film is hole doped, or when pressure is gradually applied on the bulk $\text{La}_3\text{Ni}_2\text{O}_7$ up to 30 GPa (see the blue line, green line, and raising portion of red line in Fig. 7(a)), the tuning parameter gradually shifts rightward from region I into region II, during which the d_{z^2} -orbital bonding band shifts closer to and eventually touches the Fermi energy. Concurrently, the γ pocket emerges, as shown in Fig. 7(b,c) below region II. Note that near the M point, the d_{z^2} -orbital bonding band is very flat, that is, the Fermi velocity is almost zero (also reflected in the extremely thick γ pocket in Fig. 7(b) below region II). Thus, the DOS increases as the parameter shifts from region I into region II, and reaches maximum in region II. Such a trend of DOS is consistent with other weak-coupling result [106]. When the tuning parameter shifts rightward from region II into region III, the γ pocket gradually expands. Although the length of the γ pocket increases, the Fermi velocity rises rapidly, causing the DOS to decline. Finally, from region III to region IV, the γ pocket continues to expand and the Fermi velocity rises, resulting in continuous decrease of the DOS. Experimentally, the right shift of the tuning parameters from region II to region IV is realized through either applying pressure from 30 GPa to 100 GPa on bulk $\text{La}_3\text{Ni}_2\text{O}_7$, or the Nd substitution, see the falling portion of the red line and the black line in Fig. 7(a).

We have completely demonstrated how the evolution of the FS and band structure dominates the variation in the DOS, which further leads to the same variation trend in the T_c of SC. This indicates that the FS and band structure deeply influence on the conclusions of weak-coupling studies. For example, for pressure-controlled SC in bulk $\text{La}_3\text{Ni}_2\text{O}_7$, since the adopted band structures are qualitatively identical, our RPA study and other weak-coupling studies [62, 103] give the same conclusion, which is also consistent with the experimental results. Another example is the weak-coupling study for SC in bulk $\text{La}_3\text{Ni}_2\text{O}_7$ with Nd-substitution, our RPA study and other weak-coupling study [51] adopt similar band structures and reach the same conclusion, which contradicts the experimental findings. On the contrary, since the distinctly different band structures are adopted to describe the system, some weak-coupling studies yield results different

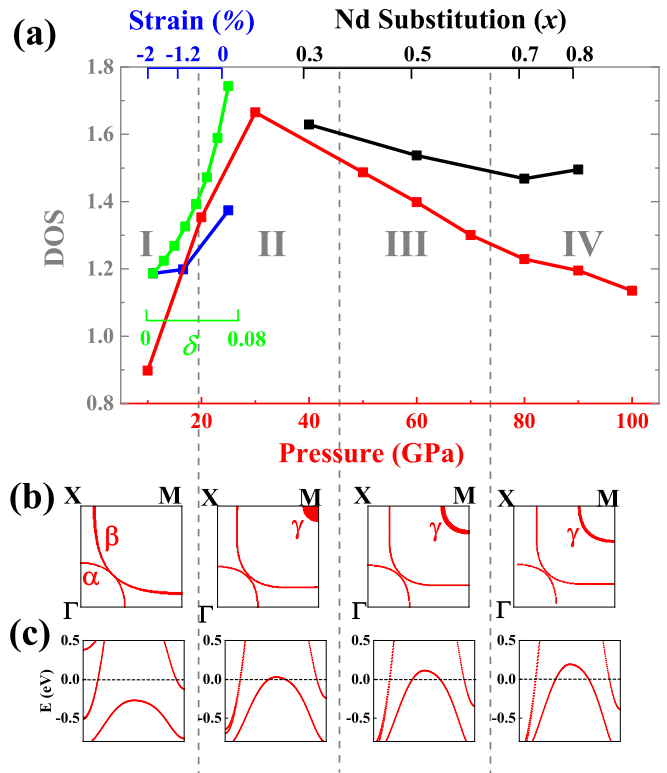


FIG. 7. (a) the DOS curves under variations in Nd-substitution (black line), pressure (red line), compressive strain (blue line), and hole doping (green line), and the corresponding horizontal coordinates adopt the same color as the DOS curves. from left to right, (a) is divided into four regions, marked by Roman numerals I~IV, and separated by gray dashed lines. (b-c) Four schematic diagram of (b) the FSs and (c) band structure near Fermi energy of the systems corresponding to the parameter points in each region. the dash lines in (c) represent Fermi energy.

from ours. For instance, several weak-coupling studies use the band with γ pocket to describe the $\text{La}_3\text{Ni}_2\text{O}_7$ thin film [105, 106]. As the compressive strain gradually increases, the γ pocket shrinks and DOS increases (corresponding to the shift from region III to region II in Fig. 7(a)). These calculation results support that compressive strain promotes the SC on the $\text{La}_3\text{Ni}_2\text{O}_7$ thin film. Furthermore, based on the band structure with γ pocket, weak-coupling study concludes that hole doping suppresses SC on the $\text{La}_3\text{Ni}_2\text{O}_7$ thin films (corresponding to the shift from region II to region III in Fig. 7(a)). These results are consistent with experimental observations but are qualitatively opposite to our results shown in Fig. 6. The conclusions of the weak coupling studies depend on the presence or absence of the γ pocket, which remains an experimental debate.

As a summary, our RPA results are only consistent with the experimental findings of pressure-controlled of T_c , while contradicting the experimental findings of other tuning parameters, including Nd-substitution, strain, and hole doping. Further analysis shows that the evo-

lution of the band structures and FS with tuning parameters determines the RPA results. Through comparisons with other weak-coupling studies, we summarize that pressure-controlled T_c in bulk $\text{La}_3\text{Ni}_2\text{O}_7$ can be well understood within the framework of weak-coupling. Whereas, the weak-coupling results consistently indicate that Nd-substitution suppresses SC. This is attributed to the larger Nd atoms reducing the Ni-Ni distance, which in turn lowers the DOS and consequently decreases T_c . Furthermore, for strain tuning and hole doping in $\text{La}_3\text{Ni}_2\text{O}_7$ thin film, the weak-coupling results are highly sensitive to the band structure, particularly to the existence of the γ pocket. Therefore, the weak-coupling study can not naturally and uniformly understand all the experimentally results in the bilayer nickelates.

VI. DISCUSSION AND CONCLUSIONS

Some theories of $\text{La}_3\text{Ni}_2\text{O}_7$ holds that the d_{z^2} orbitals dominate the SC [41–43, 61, 65]: The strong interlayer AFM superexchange J_{\perp}^z drives the d_{z^2} electrons to pair, and hybridization with the $d_{x^2-y^2}$ orbital brings about phase coherence, which combinedly lead to SC in $\text{La}_3\text{Ni}_2\text{O}_7$. We have also explored the possibility of understanding experiments from such viewpoint. For simplicity, we take a single d_{z^2} -orbital bilayer $t - J_{\parallel} - J_{\perp}$ model, with model parameters replaced by parameters corresponding to the d_{z^2} orbital. We have added an additional assumed next-nearest-neighbor (NNN) and next-next-nearest-neighbor hopping integrals (see **Appendix B** for details) to simulate the hopping acquired through a second-order process assisted via hybridization with the $d_{x^2-y^2}$ orbital [68]. Then we compare our SBMF results on this model with experiments. The biggest difficulty of these theories lies in the problem of hole doping. As the d_{z^2} orbital is nearly half-filled, we define $\delta_z \equiv 1 - n_{d_{z^2}} \ll 1$ as its hole density. As shown in Fig. 8(a), for small δ_z we have $T_{\text{BEC}} \propto \delta_z$ satisfying $T_{\text{BEC}} \ll T_{\text{pair}}$, and hence $T_c = T_{\text{BEC}} \propto \delta_z$ mimics underdoped cuprates. This SBMF result is qualitatively consistent with the DMRG result shown in Fig. 8(b) which yields that K_{SC} decreases with δ_z . Since hole doping in experiments enhances δ_z , the resultant $T_c = T_{\text{BEC}} \propto \delta_z$ will surely rise in these theories, which is in sharp contrast with experiments. Besides, these theories also cannot give a natural understanding toward the experiments which tune J_{\perp} , because $T_c = T_{\text{BEC}} \propto \delta_z$ is insensitive to J_{\perp} .

Besides T_c , the distribution of the pairing gap function on the FS also distinguishes between the weak-coupling theories and the strong-coupling theories. In strong-coupling theories, the superexchange interaction is typically very short ranged, leading to short-ranged pairing in real-space. In our $t - J_{\parallel} - J_{\perp}$ model, the pairing is dominantly limited between the same site i in the two layers. When such pairing is projected onto the FS, a nodeless s^{\pm} -wave pairing with opposite gap signs between the α and β pockets is obtained [108]. While for the weak-

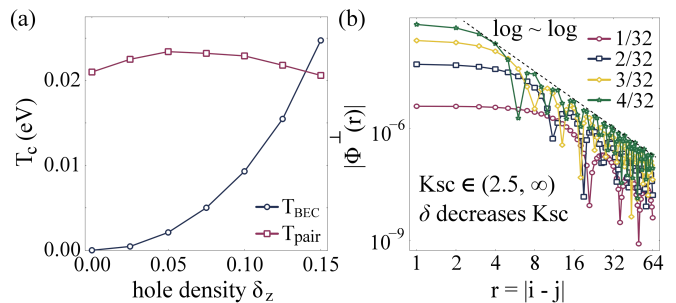


FIG. 8. Results about d_{z^2} -orbital model with different hole density level δ_z . (a) The T_{BEC} and T_{pair} (lower one as T_c) as functions of hole density calculated by SBMF theory. (b) The interlayer pairing correlation function $|\Phi^+(r)|$ with different hole density level δ calculated by DMRG.

coupling theories such as RPA [44] or FRG [35], as the effective interaction mediated by spin fluctuations is usually \mathbf{k} -space derived, the obtained distribution of the gap function on the FS is usually more continuous. As the α and β pockets hosting opposite gap signs nearly touch with each other at the diagonal direction, continuity dictates that the pairing amplitude nearly vanish along this direction, leading to a near node [35, 44]. Recent angle-resolved-photoemission-spectrum observations for the $\text{La}_3\text{Ni}_2\text{O}_7$ thin film suggest that the gap amplitude along the diagonal direction is obviously nonzero [144], supporting our strong-coupling theories.

In conclusion, based on our minimal $d_{x^2-y^2}$ -orbital bilayer $t - J_{\parallel} - J_{\perp}$ model, we have provided a unified understanding toward the series of experiments which control T_c through tuning the environment conditions. Our results suggest that, the three experimental observations, i.e. the enhancement of bulk T_c under pressure with the increase of rare-earth Sm/Nd substitution fraction, the dome shaped pressure dependence of bulk T_c and the enhancement of T_c with compressive strain in the film, all originate from the variation of the interlayer superexchange J_{\perp} with tuning parameters; and the suppression of T_c by hole doping originates from decreased filling fraction of the $d_{x^2-y^2}$ orbital which leads to reduced DOS of the $d_{x^2-y^2}$ orbital. In comparison with RPA, our strong-coupling theory provides a more natural understanding toward the series of experiments. We further predict that electron doping implemented through substitution of La by element with higher valence in pressurized bulk or compressive-strained film, or further enhancement of the compressive strain in the film, can enhance T_c .

ACKNOWLEDGMENTS

We are grateful to the stimulation discussions with Xin-Wei Yi, Wei Li and Chen Lu. This work is supported by the National Natural Science Foundation of China under the Grant Nos. 12574141, 12234016 and 12074031. Y.-B. L. is supported by the postdoctoral in-

novation talent support program (Grant No. A5B10039)

Appendix A: From the Two-orbital Model to the One-Orbital Model

We start with the two E_g -orbital bilayer $t - J - J_H$ model [37]

$$H = \mathcal{P}H_0\mathcal{P} + J_{\parallel}^x \sum_{\langle i,j \rangle, \alpha} \mathbf{S}_{i\alpha}^x \cdot \mathbf{S}_{j\alpha}^x + J_{\perp}^z \sum_i \mathbf{S}_{i1}^z \cdot \mathbf{S}_{i2}^z - 2J_H \sum_{i\alpha} \mathbf{S}_{i\alpha}^x \cdot \mathbf{S}_{i\alpha}^z, \quad (\text{S1})$$

where $\mathbf{S}_{i\alpha}^a = \frac{1}{2}c_{i\alpha\sigma}^{a\dagger}[\boldsymbol{\sigma}]_{\sigma\sigma'}c_{i\alpha\sigma'}$ is the spin operator with Pauli matrices $\boldsymbol{\sigma} = (\sigma_x, \sigma_y, \sigma_z)$ in the α -th layer ($\alpha = 1, 2$), and a represents the d_{z^2} (z) or the $d_{x^2-y^2}$ (x) orbital. \mathcal{P} is the Gutzwiller projector that excludes double occupancy in the same orbital at the same site. $\langle i, j \rangle$ represents the nearest neighbor (NN) sites within a layer. H_0 is the tight-binding Hamiltonian taking the form

$$H_0 = \sum_{i,\alpha,\sigma} (\mu_x n_{i\alpha\sigma}^x + \mu_z n_{i\alpha\sigma}^z) - \sum_{i,j,\alpha,\sigma} t_{ij}^x (c_{i\alpha\sigma}^{x\dagger} c_{j\alpha\sigma}^x + \text{h.c.}) - \sum_{i,j,\alpha,\sigma} t^{xz} (c_{i\alpha\sigma}^{z\dagger} c_{j\alpha\sigma}^x + (z \leftrightarrow x) + \text{h.c.}) - \sum_{i,\sigma} t^z (c_{i1\sigma}^{z\dagger} c_{i2\sigma}^z + \text{h.c.}). \quad (\text{S2})$$

Here, $c_{i\alpha\sigma}^{a\dagger}$ ($c_{i\alpha\sigma}^a$) creates (annihilates) a $a = z, x$ -orbital electron with spin $\sigma = \{\uparrow, \downarrow\}$ at the site i in layer $\alpha = 1, 2$, and $n_{i\alpha\sigma}^a = c_{i\alpha\sigma}^{a\dagger} c_{i\alpha\sigma}^a$ is the particle number operator. t^{xz} represents the non-zero NN hybridization between the two E_g orbitals, exhibiting opposite signs along x - and y -directions due to the symmetry constraint, $t_x^{xz} = -t_y^{xz} = t^{xz}$.

The nearly half-filled d_{z^2} -orbital electrons can be treated approximately as local spinons, and the interlayer superexchange J_{\perp}^z provides a strong antiferromagnetic (AFM) coupling. The Hund's coupling J_H drives a pair of onsite d_{z^2} -orbital and $d_{x^2-y^2}$ -orbital electrons tending to form a spin-1 doublon, thus transfers an effective interlayer superexchange to $d_{x^2-y^2}$ -orbital from J_{\perp}^z . With this, an effective one-orbital bilayer $t - J_{\parallel} - J_{\perp}$ model can be obtained [37, 38, 49, 55, 56, 59, 69, 110–112, 115–117, 120, 121]

$$H = - \sum_{i,j,\alpha,\sigma} \mathcal{P} t_{ij} (c_{i\alpha\sigma}^{\dagger} c_{j\alpha\sigma} + \text{h.c.}) \mathcal{P} + J_{\parallel} \sum_{\langle i,j \rangle, \alpha} \mathbf{S}_{i\alpha} \cdot \mathbf{S}_{j\alpha} + J_{\perp} \sum_i \mathbf{S}_{i1} \cdot \mathbf{S}_{i2}. \quad (\text{S3})$$

where $c_{i\alpha\sigma}^{(\dagger)} = c_{i\alpha\sigma}^{x(\dagger)}$, $\mathbf{S}_{i\alpha} = \mathbf{S}_{i\alpha}^x$, $t_{ij} = t_{ij}^x$, $J_{\parallel} = J_{\parallel}^x$, and J_{\perp} denote the effective superexchange interaction between layers.

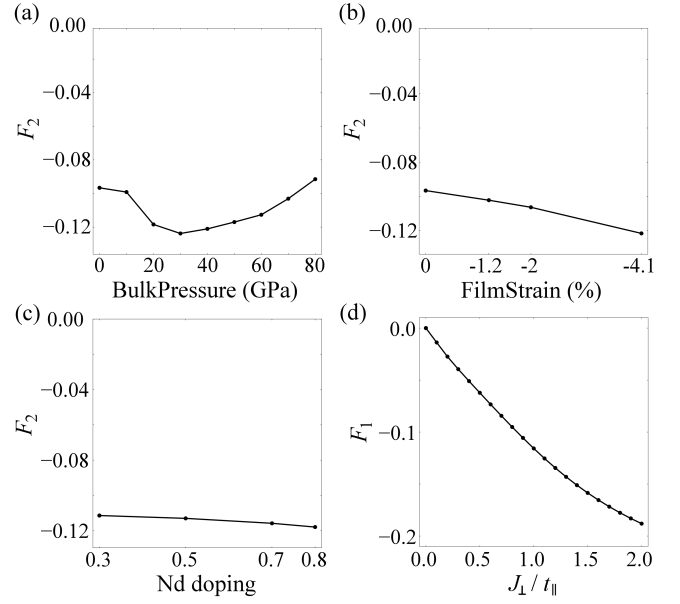


FIG. A1. (a-c) The interlayer spin order parameter F_2 changes with different parameters: The results on Nd-substitution-dependence in the bulk for (a), pressure-dependence in the bulk for (b) and strain-dependence in the film for (c). (d) The interlayer spin order parameter F_1 changes with J_{\perp}/t_{\parallel} .

We employ the density matrix renormalization group (DMRG) method [124, 145] to solve the two-orbital $t - J - J_H$ model on a $2 \times 1 \times 48$ ladder. To simplify the computation, we fix the d_{z^2} -orbital at half-filling, which degenerates the Hamiltonian (S1) into

$$H = \mu_x \sum_{i\alpha\sigma} n_{i\alpha\sigma}^x - \sum_{ij\alpha\sigma} t_{ij}^x (c_{i\alpha\sigma}^{x\dagger} c_{j\alpha\sigma}^x + \text{h.c.}) + J_{\parallel}^x \sum_{\langle i,j \rangle, \alpha} \mathbf{S}_{i\alpha}^x \cdot \mathbf{S}_{j\alpha}^x + J_{\perp}^z \sum_i \mathbf{S}_{i1}^z \cdot \mathbf{S}_{i2}^z - 2J_H \sum_{i\alpha} \mathbf{S}_{i\alpha}^x \cdot \mathbf{S}_{i\alpha}^z. \quad (\text{S4})$$

We calculate the interlayer spin order parameter $F_2 = \sum_i \langle \mathbf{S}_{i1}^x \cdot \mathbf{S}_{i2}^x \rangle / N$ in different situations to characterize the strength of the AFM correlation between layers in $d_{x^2-y^2}$ -orbital transferred from d_{z^2} -orbital. The results are shown in Fig. A1 (a-c).

We also solve the one-orbital model (S3) on a $2 \times 2 \times 24$ lattice by DMRG and calculate the interlayer spin order parameter $F_1 = \sum_i \langle \mathbf{S}_{i1} \cdot \mathbf{S}_{i2} \rangle / N$ to match F_2 from the two-orbital model.

We adjust J_{\perp} in the one-orbital model to control F_1 , as shown in Fig. A1 (d). J_{\perp} which takes $F_1 = F_2$ is considered the effective superexchange parameter transferred from J_{\perp}^z , and the transfer ratio is $\eta = J_{\perp}/J_{\perp}^z$.

Appendix B: Slave-Boson Mean-Field Treatment of the One-Orbital Model

We start from a general $t - J_{\parallel} - J_{\perp}$ model of the $d_{x^2-y^2}$ orbital or the d_{z^2} orbital:

$$\begin{aligned}
H_a = & - \sum_{i,j,\alpha,\sigma} \mathcal{P} t_{ij}^a \left(c_{i\alpha\sigma}^a \dagger c_{j\alpha\sigma}^a + h.c. \right) \mathcal{P} \\
& - t_{\perp}^a \sum_{i\sigma} \left(c_{i1\sigma}^a \dagger c_{i2\sigma}^a + h.c. \right) \\
& + J_{\parallel}^a \sum_{\langle i,j \rangle, \alpha} \mathbf{S}_{i\alpha}^a \cdot \mathbf{S}_{j\alpha}^a + J_{\perp}^a \sum_i \mathbf{S}_{i1}^a \cdot \mathbf{S}_{i2}^a.
\end{aligned} \tag{S5}$$

Here, a represents d_{z^2} or $d_{x^2-y^2}$ orbital.

In SBMF theory, we have $c_{i\alpha\sigma}^{\dagger} = f_{i\alpha\sigma}^{\dagger} b_{i\alpha}$, and $f_{i\alpha\sigma}^{\dagger}$ is the spinon creation operator, $b_{i\alpha}$ is the holon annihilation operator. SC is satisfied by pairing of spinons and condensation of holons. The local Hilbert space excludes the double occupancy, so there is the constraint by $\sum_{\sigma} f_{i\alpha\sigma}^{\dagger} f_{i\alpha\sigma} + b_{i\alpha}^{\dagger} b_{i\alpha} = 1$. In our calculation, we focus on the effects of J_{\perp} and the filling fraction n on the interlayer pairing Δ of the $d_{x^2-y^2}$ orbital, so we set $J_{\parallel} = 0$. By defining the order parameters:

$$\begin{aligned}
\chi_{\parallel\alpha}^* &= \frac{1}{2N} \sum_{\langle i,j \rangle, \sigma} f_{i\alpha\sigma}^{\dagger} f_{j\alpha\sigma}, \\
\chi_{\perp}^* &= \frac{1}{N} \sum_{i\sigma} f_{i1\sigma}^{\dagger} f_{i2\sigma}, \\
\Delta^* &= \frac{1}{N} \sum_i f_{i1\uparrow}^{\dagger} f_{i2\downarrow}^{\dagger} - f_{i1\downarrow}^{\dagger} f_{i2\uparrow}^{\dagger},
\end{aligned} \tag{S6}$$

we get the mean-field Hamiltonian of the $d_{x^2-y^2}$ orbital:

$$\begin{aligned}
H_{MF}^x = & \sum_{i,j,\alpha} \left(-t_{ij} b_{i\alpha} b_{j\alpha}^{\dagger} \sum_{\sigma} f_{i\alpha\sigma}^{\dagger} f_{j\alpha\sigma} + h.c. \right) \\
& - t_{\perp} \sum_i \left(b_{i1} b_{i2}^{\dagger} \sum_{\sigma} f_{i1\sigma}^{\dagger} f_{i2\sigma} + h.c. \right) \\
& - \frac{3}{8} J_{\perp} \chi_{\perp} \sum_i \left(f_{i1\uparrow}^{\dagger} f_{i2\uparrow}^{\dagger} + f_{i1\downarrow}^{\dagger} f_{i2\downarrow}^{\dagger} \right) + h.c. \\
& - \frac{3}{8} J_{\perp} \Delta \sum_i \left(f_{i1\uparrow}^{\dagger} f_{i2\downarrow}^{\dagger} - f_{i1\downarrow}^{\dagger} f_{i2\uparrow}^{\dagger} \right) + h.c. \\
& + \sum_{i\alpha} \lambda_{i\alpha} \left(\sum_{\sigma} f_{i\alpha\sigma}^{\dagger} f_{i\alpha\sigma} + b_{i\alpha}^{\dagger} b_{i\alpha} - 1 \right) + \text{const.}
\end{aligned} \tag{S7}$$

The mean-field Hamiltonian can be separated by spinon H_s and holon H_b parts $H_{MF} = H_f + H_b$. For the spinon part, the holon is condensed and the holon operator is simply replaced by a number $b_{i\alpha} = b_{i\alpha}^{\dagger} = \sqrt{\delta_{i\alpha}}$, and $\delta =$

$1 - 2n$ in which n is the filling fraction. We get

$$\begin{aligned}
H_f = & \sum_{\mathbf{k}\alpha\sigma} \varepsilon_{\mathbf{k}\alpha} f_{\mathbf{k}\alpha\sigma}^{\dagger} f_{\mathbf{k}\alpha\sigma} \\
& - \left(\frac{3}{8} J_{\perp} \chi_{\perp} + t_{\perp} \delta \right) \sum_{\mathbf{k}} \left[\left(f_{\mathbf{k}1\uparrow}^{\dagger} f_{\mathbf{k}2\uparrow}^{\dagger} + f_{-\mathbf{k}1\downarrow}^{\dagger} f_{-\mathbf{k}2\downarrow}^{\dagger} \right) + h.c. \right] \\
& - \frac{3}{8} J_{\perp} \Delta \sum_{\mathbf{k}} \left[\left(f_{\mathbf{k}1\uparrow}^{\dagger} f_{-\mathbf{k}2\downarrow}^{\dagger} - f_{-\mathbf{k}1\downarrow}^{\dagger} f_{\mathbf{k}2\uparrow}^{\dagger} \right) + h.c. \right] + \text{const},
\end{aligned} \tag{S8}$$

in which $\varepsilon_{\mathbf{k}\alpha} = \varepsilon_{\mathbf{k}} = -2t_{\parallel} \delta (\cos k_x + \cos k_y) - 4t_2 \delta \cos k_x \cos k_y - 2t_3 \delta (\cos 2k_x + \cos 2k_y) - \mu_f$, t_{\parallel} is the intralayer NN hopping, t_2 is the intralayer next nearest neighbor (NNN) hopping, and t_3 is the intralayer third-nearest neighbor hopping. By introducing the Nambu spinor $\psi_{\mathbf{k}}^{\dagger} = (f_{\mathbf{k}1\uparrow}^{\dagger} f_{\mathbf{k}2\uparrow}^{\dagger} f_{-\mathbf{k}1\downarrow} f_{-\mathbf{k}2\downarrow})$, the Hamiltonian

$$\begin{aligned}
H_f = & \sum_{\mathbf{k}} \psi_{\mathbf{k}}^{\dagger} \begin{pmatrix} \varepsilon_{\mathbf{k}} & -\tilde{t}_{\perp} & 0 & -\frac{3}{8} J_{\perp} \Delta \\ -\tilde{t}_{\perp} & \varepsilon_{\mathbf{k}} & -\frac{3}{8} J_{\perp} \Delta & 0 \\ 0 & -\frac{3}{8} J_{\perp} \Delta & -\varepsilon_{\mathbf{k}} & \tilde{t}_{\perp} \\ -\frac{3}{8} J_{\perp} \Delta & 0 & \tilde{t}_{\perp} & -\varepsilon_{\mathbf{k}} \end{pmatrix} \psi_{\mathbf{k}} \\
& + \text{const}
\end{aligned} \tag{S9}$$

($\tilde{t}_{\perp} = 3/8 J_{\perp} \chi_{\perp} + t_{\perp} \delta$) can be diagonalized through a unitary transformation:

$$\begin{aligned}
H_f = & \sum_{\mathbf{k}} \psi_{\mathbf{k}}^{\dagger} U_{\mathbf{k}} U_{\mathbf{k}}^{-1} H_{\mathbf{k}} U_{\mathbf{k}} U_{\mathbf{k}}^{-1} \psi_{\mathbf{k}} + \text{const} \\
= & \sum_{\mathbf{k}} \gamma_{\mathbf{k}}^{\dagger} E_{\mathbf{k}} \gamma_{\mathbf{k}} + \text{const},
\end{aligned} \tag{S10}$$

here $\gamma_{\mathbf{k}}^{\dagger} = \psi_{\mathbf{k}}^{\dagger} U_{\mathbf{k}}$ and $E_{\mathbf{k}} = U_{\mathbf{k}}^{-1} H_{\mathbf{k}} U_{\mathbf{k}}$ in which there are eigenvalues $E_{\mathbf{k}\beta}$ ($\beta = 1, 2, 3, 4$).

In SBMF theory, we solve the self-consistent equations of order parameters:

$$\begin{aligned}
\langle \chi_{\perp} \rangle &= \frac{1}{N} \sum_{\mathbf{k}\sigma} \langle f_{\mathbf{k}1\sigma}^{\dagger} f_{\mathbf{k}2\sigma} \rangle, \\
\langle \chi_{\parallel\alpha} \rangle &= \frac{1}{N} \sum_{\mathbf{k}\sigma} \frac{\cos k_x + \cos k_y}{2} \langle f_{\mathbf{k}\alpha\sigma}^{\dagger} f_{\mathbf{k}\alpha\sigma} \rangle, \\
\langle \Delta \rangle^* &= \frac{2}{N} \sum_{\mathbf{k}} \langle f_{\mathbf{k}1\uparrow}^{\dagger} f_{-\mathbf{k}2\downarrow}^{\dagger} \rangle, \\
n &= \frac{1}{2N} \sum_{\mathbf{k}\sigma} \left(\langle f_{\mathbf{k}1\sigma}^{\dagger} f_{\mathbf{k}1\sigma} \rangle + \langle f_{\mathbf{k}2\sigma}^{\dagger} f_{\mathbf{k}2\sigma} \rangle \right).
\end{aligned} \tag{S11}$$

by changing it to $\langle \gamma_{\mathbf{k}\beta}^{\dagger} \gamma_{\mathbf{k}\beta} \rangle$ through the above unitary transformation $\psi_{\mathbf{k}}^{\dagger} = \gamma_{\mathbf{k}}^{\dagger} U^{-1}$, and the quasi-particle satisfies the Fermi-Dirac distribution function $\langle \gamma_{\mathbf{k}\beta}^{\dagger} \gamma_{\mathbf{k}\beta} \rangle = f(E_{\mathbf{k}\beta}) = \frac{1}{e^{E_{\mathbf{k}\beta}/T} + 1}$. The iteration continues until the errors of these parameters converge to 10^{-8} . In the calculation of finite temperature, we set different temperatures to find the point when $\Delta \rightarrow 0$ to obtain T_{pair} . The calculation of the d_{z^2} orbital is similar with above process.

Next we introduce the calculation of T_{BEC} by the holon part Hamiltonian:

$$\begin{aligned}
H_b &= \sum_{i,j,\alpha,\sigma} -t_{ij} b_{i\alpha} b_{j\alpha}^\dagger \langle f_{i\alpha\sigma}^\dagger f_{j\alpha\sigma} \rangle + h.c. \\
&\quad - t_\perp \sum_{i\sigma} b_{i1} b_{i2}^\dagger \langle f_{i1\sigma}^\dagger f_{i2\sigma} \rangle + h.c. \\
&= \sum_{i,j,\alpha,\sigma} \left(-t_{ij} \chi_{ij} b_{i\alpha} b_{j\alpha}^\dagger + h.c. \right) \\
&\quad - t_\perp \sum_{i\sigma} \left(\chi_{\perp i} b_{i1} b_{i2}^\dagger + h.c. \right)
\end{aligned} \tag{S12}$$

As a two-dimensional system, T_{BEC} of holon is decided by the Kosterlitz-Thouless (KT) transition. First we consider a tight-binding model in the 2D square lattice with NN hopping, and the phase fluctuations at finite temperature, there is $b_i = \sqrt{\delta} e^{i\theta_i}$, and

$$\begin{aligned}
H_b &= -t\delta \sum_{ij} e^{i(\theta_i - \theta_j)} + h.c. = -t\delta \sum_{ij} 2 \cos(\theta_i - \theta_j) \\
&= t\delta \sum_{ij} (\theta_i - \theta_j)^2 + \text{const} = t\delta \sum_i |\nabla\theta_i|^2 a^2 + \text{const} \\
&\equiv \int \rho |\nabla\theta|^2 d^2\mathbf{r} + \text{const},
\end{aligned} \tag{S13}$$

in which $\rho = t\delta$ is the superfluid density which represents the phase stiffness. T_{BEC} is calculated by the Kosterlitz-Thouless (KT) transition:

$$T_{\text{BEC}} = T_{\text{KT}} = \frac{\pi}{2} \rho = \frac{\pi}{2} t\delta \tag{S14}$$

For the $d_{x^2-y^2}$ orbital, the interlayer hopping t_\perp^x is small that can be ignored. So,

$$\begin{aligned}
H_b^x &= \delta \sum_i \tilde{t}_\parallel |\nabla\theta_i|^2 a^2 + \tilde{t}_2 |\nabla\theta_i|^2 2a^2 + \tilde{t}_3 |\nabla\theta_i|^2 4a^2 \\
&\equiv \int \rho |\nabla\theta|^2 d^2\mathbf{r}
\end{aligned} \tag{S15}$$

in which $\rho = \tilde{t}_\parallel \delta + 2\tilde{t}_2 \delta + 4\tilde{t}_3 \delta$, and

$$T_{\text{BEC}} = \frac{\pi}{2} \rho. \tag{S16}$$

For the d_{z^2} orbital, there is something different that the interlayer hopping is much larger than the intralayer hopping, and lead to the bonding state and the anti-bonding state:

$$\begin{aligned}
H_b^z &= - \sum_{i\alpha\mathbf{r}} t_\mathbf{r}^z \left(b_{i\alpha}^\dagger b_{i+\mathbf{r}\alpha} + h.c. \right) - \sum_i t_\perp^z \left(b_{i1}^\dagger b_{i2} + h.c. \right) \\
&= - \sum_{i\alpha\mathbf{r}} t_\mathbf{r}^z \left(b_{i+}^\dagger b_{i+\mathbf{r}+} + b_{i-}^\dagger b_{i+\mathbf{r}-} \right) + h.c. \\
&\quad - \sum_i t_\perp^z \left(b_{i+}^\dagger b_{i+} - b_{i-}^\dagger b_{i-} \right)
\end{aligned} \tag{S17}$$

in which $b_{i+}^\dagger = (b_{i1}^\dagger + b_{i2}^\dagger) / \sqrt{2}$ is the bonding state operator, and $b_{i-}^\dagger = (b_{i1}^\dagger - b_{i2}^\dagger) / \sqrt{2}$ is the anti-bonding operator. When BEC happens, particles condense at the bonding state which has lower energy, and the filling fraction of holon becomes $\tilde{\delta} = 2\delta$. So

$$H_b^z = \int \tilde{\rho} |\nabla\theta_+|^2 d^2\mathbf{r} \tag{S18}$$

in which $\tilde{\rho} = \tilde{t}_1^z \cdot 2\delta + \tilde{t}_2^z \cdot 4\delta + \tilde{t}_3^z \cdot 8\delta + \dots$. And $T_{\text{BEC}} = \frac{\pi}{2} \tilde{\rho}$. As the assumption of Refs.[41] that SC is caused by pair of d_{z^2} orbital electrons and coherence by hybridization of the $d_{x^2-y^2}$ and d_{z^2} orbital, we $\tilde{t}_1^z = t_1^z \chi_\parallel$ set $\tilde{t}_2 = 0.2$ and $\tilde{t}_3 = 0.1$ as reasonable values.

- [1] H. Sun, M. Huo, X. Hu, J. Li, Z. Liu, Y. Han, L. Tang, Z. Mao, P. Yang, B. Wang, J. Cheng, D.-X. Yao, G.-M. Zhang, and M. Wang, Signatures of superconductivity near 80 K in a nickelate under high pressure, *Nature* **621**, 493 (2023).
- [2] Y. Zhang, D. Su, Y. Huang, Z. Shan, H. Sun, M. Huo, K. Ye, J. Zhang, Z. Yang, Y. Xu, Y. Su, R. Li, M. Smidman, M. Wang, L. Jiao, and H. Yuan, Superconductivity with high critical temperature with zero resistance and strange-metal behaviour in $\text{La}_3\text{Ni}_2\text{O}_{7-\delta}$, *Nat. Phys.* **20**, 1269 (2024).
- [3] J. Hou, P.-T. Yang, Z.-Y. Liu, J.-Y. Li, P.-F. Shan, L. Ma, G. Wang, N.-N. Wang, H.-Z. Guo, J.-P. Sun, Y. Uwatoko, M. Wang, G.-M. Zhang, B.-S. Wang, and J.-G. Cheng, Emergence of superconductivity with high critical temperature in pressurized $\text{La}_3\text{Ni}_2\text{O}_7$ crystals, *Chin. Phys. Lett.* **40**, 117302 (2023).
- [4] G. Wang, N. N. Wang, X. L. Shen, J. Hou, L. Ma, L. F. Shi, Z. A. Ren, Y. D. Gu, H. M. Ma, P. T. Yang, Z. Y. Liu, H. Z. Guo, J. P. Sun, G. M. Zhang, S. Calder, J.-Q. Yan, B. S. Wang, Y. Uwatoko, and J.-G. Cheng, Pressure-induced superconductivity in polycrystalline $\text{La}_3\text{Ni}_2\text{O}_7$, *Phys. Rev. X* **14**, 011040 (2024).
- [5] Y. Zhou, J. Guo, S. Cai, H. Sun, C. Li, J. Zhao, P. Wang, J. Han, X. Chen, Y. Chen, Q. Wu, Y. Ding, T. Xiang, H.-k. Mao, and L. Sun, Investigations of key issues on the reproducibility of high- T_c superconductivity emerging from compressed $\text{La}_3\text{Ni}_2\text{O}_7$, *Matter and Radiation at Extremes* **10**, 027801 (2025).
- [6] M. Zhang, C. Pei, Q. Wang, Y. Zhao, C. Li, W. Cao, S. Zhu, J. Wu, and Y. Qi, Effects of pressure and doping on ruddlesden-popper phases $\text{La}_{n+1}\text{Ni}_n\text{O}_{3n+1}$, *J. Mater. Sci. Technol.* **185**, 147 (2024).
- [7] L. Wang, Y. Li, S. Xie, F. Liu, H. Sun, C. Huang, Y. Gao, T. Nakagawa, B. Fu, B. Dong, Z. Cao, R. Yu, S. I. Kawaguchi, H. Kadobayashi, M. Wang, C. Jin, H. kwang Mao, and H. Liu, Structure responsible for the superconducting state in $\text{La}_3\text{Ni}_2\text{O}_7$ at low temperature and high pressure conditions, *Journal of the American Chemical Society* **146**, 7506 (2024).
- [8] J. Li, D. Peng, P. Ma, H. Zhang, Z. Xing, X. Huang, C. Huang, M. Huo, D. Hu, Z. Dong, X. Chen, T. Xie, H. Dong, H. Sun, Q. Zeng, H.-k. Mao, and M. Wang, Identification of superconductivity in bilayer nickelate $\text{La}_3\text{Ni}_2\text{O}_7$ under high pressure up to 100 Gpa, *National Science Review*, nwaf220 (2025).
- [9] Z. Dong, M. Huo, J. Li, J. Li, P. Li, H. Sun, L. Gu, Y. Lu, M. Wang, Y. Wang, and Z. Chen, Visualization of oxygen vacancies and self-doped ligand holes in $\text{La}_3\text{Ni}_2\text{O}_{7-\delta}$, *Nature* **630**, 847 (2024).
- [10] N. Wang, G. Wang, X. Shen, J. Hou, J. Luo, X. Ma, H. Yang, L. Shi, J. Dou, J. Feng, J. Yang, Y. Shi, Z. Ren, H. Ma, P. Yang, Z. Liu, Y. Liu, H. Zhang, X. Dong, Y. Wang, K. Jiang, J. Hu, S. Nagasaki, K. Kitagawa, S. Calder, J. Yan, J. Sun, B. Wang, R. Zhou, Y. Uwatoko, and J. Cheng, Bulk superconductivity with high critical temperature in pressurized tetragonal $\text{La}_2\text{PrNi}_2\text{O}_7$, *Nature* **634**, 579 (2024).
- [11] Y. Zhu, D. Peng, E. Zhang, B. Pan, X. Chen, L. Chen, H. Ren, F. Liu, Y. Hao, N. Li, et al., Superconductivity in pressurized trilayer $\text{La}_4\text{Ni}_3\text{O}_{10-\delta}$ single crystals, *Nature* **631**, 531 (2024).
- [12] Q. Li, Y.-J. Zhang, Z.-N. Xiang, Y. Zhang, X. Zhu, and H.-H. Wen, Signature of superconductivity in pressurized $\text{La}_4\text{Ni}_3\text{O}_{10}$, *Chin. Phys. Lett.* **41**, 017401 (2024).
- [13] M. Zhang, C. Pei, D. Peng, X. Du, W. Hu, Y. Cao, Q. Wang, J. Wu, Y. Li, H. Liu, C. Wen, J. Song, Y. Zhao, C. Li, W. Cao, S. Zhu, Q. Zhang, N. Yu, P. Cheng, L. Zhang, Z. Li, J. Zhao, Y. Chen, C. Jin, H. Guo, C. Wu, F. Yang, Q. Zeng, S. Yan, L. Yang, and Y. Qi, Superconductivity in trilayer nickelate $\text{La}_4\text{Ni}_3\text{O}_{10}$ under pressure, *Phys. Rev. X* **15**, 021005 (2025).
- [14] M. Shi, D. Peng, K. Fan, Z. Xing, S. Yang, Y. Wang, H. Li, R. Wu, M. Du, B. Ge, Z. Zeng, Q. Zeng, J. Ying, T. Wu, and X. Chen, Pressure induced superconductivity in hybrid ruddlesden-popper $\text{La}_5\text{Ni}_3\text{O}_{11}$ single crystals, *Nature Physics* **21**, 1780 (2025).
- [15] P. Puphal, P. Reiss, N. Enderlein, Y.-M. Wu, G. Khalullin, V. Sundaramurthy, T. Priessnitz, M. Knauff, A. Suthar, L. Richter, M. Isobe, P. A. van Aken, H. Takagi, B. Keimer, Y. E. Suyolcu, B. Wehinger, P. Hansmann, and M. Hepting, Unconventional crystal structure of the high-pressure superconductor $\text{La}_3\text{Ni}_2\text{O}_7$, *Phys. Rev. Lett.* **133**, 146002 (2024).
- [16] S. Abadi, K.-J. Xu, E. G. Lomeli, P. Puphal, M. Isobe, Y. Zhong, A. V. Fedorov, S.-K. Mo, M. Hashimoto, D.-H. Lu, B. Moritz, B. Keimer, T. P. Devereaux, M. Hepting, and Z.-X. Shen, Electronic structure of the alternating monolayer-trilayer phase of $\text{La}_3\text{Ni}_2\text{O}_7$, *Phys. Rev. Lett.* **134**, 126001 (2025).
- [17] Z. Liu, H. Sun, M. Huo, X. Ma, Y. Ji, E. Yi, L. Li, H. Liu, J. Yu, Z. Zhang, et al., Evidence for charge and spin density waves in single crystals of $\text{La}_3\text{Ni}_2\text{O}_7$ and $\text{La}_3\text{Ni}_2\text{O}_6$, *Sci. China Phys. Mech. Astron.* **66**, 217411 (2023).
- [18] X. Chen, J. Choi, Z. Jiang, J. Mei, K. Jiang, J. Li, S. Agrestini, M. Garcia-Fernandez, X. Huang, H. Sun, D. Shen, M. Wang, J. Hu, Y. Lu, K.-J. Zhou, and D. Feng, Electronic and magnetic excitations in $\text{La}_3\text{Ni}_2\text{O}_7$, *Nature Communications* **15**, 9597 (2024).
- [19] T. Xie, M. Huo, X. Ni, F. Shen, X. Huang, H. Sun, H. C. Walker, D. Adroja, D. Yu, B. Shen, L. He, K. Cao, and M. Wang, Strong interlayer magnetic exchange coupling in $\text{La}_3\text{Ni}_2\text{O}_{7-\delta}$ revealed by inelastic neutron scattering, *Sci. Bull.* **69**, 3221 (2024).
- [20] J.-J. Feng, T. Han, J.-P. Song, M.-S. Long, X.-Y. Hou, C.-J. Zhang, Q.-G. Mu, and L. Shan, Unaltered density wave transition and pressure-induced signature of superconductivity in Nd-doped $\text{La}_3\text{Ni}_2\text{O}_7$, *Phys. Rev. B* **110**, L100507 (2024).
- [21] Y. Meng, Y. Yang, H. Sun, S. Zhang, J. Luo, L. Chen, X. Ma, M. Wang, F. Hong, X. Wang, and X. Yu, Density-wave-like gap evolution in $\text{La}_3\text{Ni}_2\text{O}_7$ under high pressure revealed by ultrafast optical spectroscopy, *Nat. Commun.* **15**, 10408 (2024).
- [22] S. Fan, Z. Luo, M. Huo, Z. Wang, H. Li, H. Yang, M. Wang, D.-X. Yao, and H.-H. Wen, Tunneling spectra with gaplike features observed in nickelate $\text{La}_3\text{Ni}_2\text{O}_7$ at ambient pressure, *Phys. Rev. B* **110**, 134520 (2024).
- [23] Y. Li, Y. Cao, L. Liu, P. Peng, H. Lin, C. Pei, M. Zhang, H. Wu, X. Du, W. Zhao, K. Zhai, X. Zhang, J. Zhao, M. Lin, P. Tan, Y. Qi, G. Li, H. Guo, L. Yang, and

- L. Yang, Distinct ultrafast dynamics of bilayer and trilayer nickelate superconductors regarding the density-wave-like transitions, *Sci. Bull.* **70**, 180 (2024).
- [24] Z. Liu, M. Huo, J. Li, Q. Li, Y. Liu, Y. Dai, X. Zhou, J. Hao, Y. Lu, M. Wang, and H.-H. Wen, Electronic correlations and partial gap in the bilayer nickelate $\text{La}_3\text{Ni}_2\text{O}_7$, *Nat. Commun.* **15**, 7570 (2024).
- [25] M. Wang, H.-H. Wen, T. Wu, D.-X. Yao, and T. Xiang, Normal and superconducting properties of $\text{La}_3\text{Ni}_2\text{O}_7$, *Chin. Phys. Lett.* **41**, 077402 (2024).
- [26] J. Yang, H. Sun, X. Hu, Y. Xie, T. Miao, H. Luo, H. Chen, B. Liang, W. Zhu, G. Qu, et al., Orbital-dependent electron correlation in double-layer nickelate $\text{La}_3\text{Ni}_2\text{O}_7$, *Nat. Commun.* **15**, 4373 (2024).
- [27] Y. Li, X. Du, Y. Cao, C. Pei, M. Zhang, W. Zhao, K. Zhai, R. Xu, Z. Liu, Z. Li, J. Zhao, G. Li, Y. Qi, H. Guo, Y. Chen, and L. Yang, Electronic correlation and pseudogap-like behavior of superconductor with high critical temperature $\text{La}_3\text{Ni}_2\text{O}_7$, *Chin. Phys. Lett.* **41**, 087402 (2024).
- [28] Y. Liu, M. Ou, H. Chu, H. Yang, Q. Li, Y.-J. Zhang, and H.-H. Wen, Growth and characterization of the $\text{La}_3\text{Ni}_2\text{O}_{7-\delta}$ thin films: Dominant contribution of the $d_{x^2-y^2}$ orbital at ambient pressure, *Phys. Rev. Mater.* **8**, 124801 (2024).
- [29] K. Chen, X. Liu, J. Jiao, M. Zou, C. Jiang, X. Li, Y. Luo, Q. Wu, N. Zhang, Y. Guo, and L. Shu, Evidence of spin density waves in $\text{La}_3\text{Ni}_2\text{O}_{7-\delta}$, *Phys. Rev. Lett.* **132**, 256503 (2024).
- [30] N. K. Gupta, R. Gong, Y. Wu, M. Kang, C. T. Parzyck, B. Z. Gregory, N. Costa, R. Sutarto, S. Sarker, A. Singer, D. G. Schlom, K. M. Shen, and D. G. Hawthorn, Anisotropic spin stripe domains in bilayer $\text{La}_3\text{Ni}_2\text{O}_7$, *Nature Communications* **16**, 6560 (2025).
- [31] B. Chen, H. Zhang, J. Li, D. Hu, M. Huo, S. Wang, C. Xi, Z. Wang, H. Sun, M. Wang, and B. Shen, Unveiling the multiband metallic nature of the normal state in the nickelate $\text{La}_3\text{Ni}_2\text{O}_7$, *Phys. Rev. B* **111**, 054519 (2025).
- [32] M. Shi, D. Peng, Y. Li, S. Yang, Z. Xing, Y. Wang, K. Fan, H. Li, R. Wu, B. Ge, Z. Zeng, Q. Zeng, J. Ying, T. Wu, and X. Chen, Spin density wave rather than tetragonal structure is prerequisite for superconductivity in $\text{La}_3\text{Ni}_2\text{O}_{7-\delta}$, *Nature Communications* **16**, 9141 (2025).
- [33] Z. Luo, X. Hu, M. Wang, W. Wú, and D.-X. Yao, Bilayer two-orbital model of $\text{La}_3\text{Ni}_2\text{O}_7$ under pressure, *Phys. Rev. Lett.* **131**, 126001 (2023).
- [34] D. A. Shilenko and I. V. Leonov, Correlated electronic structure, orbital-selective behavior, and magnetic correlations in double-layer $\text{La}_3\text{Ni}_2\text{O}_7$ under pressure, *Phys. Rev. B* **108**, 125105 (2023).
- [35] Q.-G. Yang, D. Wang, and Q.-H. Wang, Possible s_{\pm} -wave superconductivity in $\text{La}_3\text{Ni}_2\text{O}_7$, *Phys. Rev. B* **108**, L140505 (2023).
- [36] V. Christiansson, F. Petocchi, and P. Werner, Correlated electronic structure of $\text{La}_3\text{Ni}_2\text{O}_7$ under pressure, *Phys. Rev. Lett.* **131**, 206501 (2023).
- [37] C. Lu, Z. Pan, F. Yang, and C. Wu, Interlayer-coupling-driven superconductivity with high critical temperature in $\text{La}_3\text{Ni}_2\text{O}_7$ under pressure, *Phys. Rev. Lett.* **132**, 146002 (2024).
- [38] H. Oh and Y.-H. Zhang, Type-II t - J model and shared superexchange coupling from hund's rule in superconducting $\text{La}_3\text{Ni}_2\text{O}_7$, *Phys. Rev. B* **108**, 174511 (2023).
- [39] Y. Zhang, L.-F. Lin, A. Moreo, and E. Dagotto, Electronic structure, dimer physics, orbital-selective behavior, and magnetic tendencies in the bilayer nickelate superconductor $\text{La}_3\text{Ni}_2\text{O}_7$ under pressure, *Phys. Rev. B* **108**, L180510 (2023).
- [40] J. Huang, Z. D. Wang, and T. Zhou, Impurity and vortex states in the bilayer superconductor $\text{La}_3\text{Ni}_2\text{O}_7$ with high critical temperature, *Phys. Rev. B* **108**, 174501 (2023).
- [41] Y.-F. Yang, G.-M. Zhang, and F.-C. Zhang, Interlayer valence bonds and two-component theory for high- T_c superconductivity of $\text{La}_3\text{Ni}_2\text{O}_7$ under pressure, *Phys. Rev. B* **108**, L201108 (2023).
- [42] Y. Shen, M. Qin, and G.-M. Zhang, Effective bilayer model hamiltonian and density-matrix renormalization group study for the high- T_c superconductivity in $\text{La}_3\text{Ni}_2\text{O}_7$ under high pressure, *Chinese Physics Letters* **40**, 127401 (2023).
- [43] Q. Qin and Y.-F. Yang, High- T_c superconductivity by mobilizing local spin singlets and possible route to higher T_c in pressurized $\text{La}_3\text{Ni}_2\text{O}_7$, *Phys. Rev. B* **108**, L140504 (2023).
- [44] Y.-B. Liu, J.-W. Mei, F. Ye, W.-Q. Chen, and F. Yang, s^{\pm} -wave pairing and the destructive role of apical-oxygen deficiencies in $\text{La}_3\text{Ni}_2\text{O}_7$ under pressure, *Phys. Rev. Lett.* **131**, 236002 (2023).
- [45] F. Lechermann, J. Gondolf, S. Bötzel, and I. M. Eremin, Electronic correlations and superconducting instability in $\text{La}_3\text{Ni}_2\text{O}_7$ under high pressure, *Phys. Rev. B* **108**, L201121 (2023).
- [46] H. Sakakibara, N. Kitamine, M. Ochi, and K. Kuroki, Possible high T_c superconductivity in $\text{La}_3\text{Ni}_2\text{O}_7$ under high pressure through manifestation of a nearly half-filled bilayer Hubbard model, *Phys. Rev. Lett.* **132**, 106002 (2024).
- [47] Y. Gu, C. Le, Z. Yang, X. Wu, and J. Hu, Effective model and pairing tendency in the bilayer Ni-based superconductor $\text{La}_3\text{Ni}_2\text{O}_7$, *Phys. Rev. B* **111**, 174506 (2025).
- [48] Z. Liao, L. Chen, G. Duan, Y. Wang, C. Liu, R. Yu, and Q. Si, Electron correlations and superconductivity in $\text{La}_3\text{Ni}_2\text{O}_7$ under pressure tuning, *Phys. Rev. B* **108**, 214522 (2023).
- [49] X.-Z. Qu, D.-W. Qu, J. Chen, C. Wu, F. Yang, W. Li, and G. Su, Bilayer t - J - J_{\perp} model and magnetically mediated pairing in the pressurized nickelate $\text{La}_3\text{Ni}_2\text{O}_7$, *Phys. Rev. Lett.* **132**, 036502 (2024).
- [50] K. Jiang, Z. Wang, and F.-C. Zhang, Superconductivity with high critical temperature in $\text{La}_3\text{Ni}_2\text{O}_7$, *Chin. Phys. Lett.* (2023).
- [51] Y. Zhang, L.-F. Lin, A. Moreo, T. A. Maier, and E. Dagotto, Trends in electronic structures and s_{\pm} -wave pairing for the rare-earth series in bilayer nickelate superconductor $\text{R}_3\text{Ni}_2\text{O}_7$, *Phys. Rev. B* **108**, 165141 (2023).
- [52] X.-Z. Qu, D.-W. Qu, X.-W. Yi, W. Li, and G. Su, Hund's rule, interorbital hybridization, and high- T_c superconductivity in the bilayer nickelate $\text{La}_3\text{Ni}_2\text{O}_7$, *Phys. Rev. B* **112**, L161101 (2025).
- [53] R. Jiang, J. Hou, Z. Fan, Z.-J. Lang, and W. Ku, Pressure driven fractionalization of ionic spins results in cupratelike high- T_c superconductivity in $\text{La}_3\text{Ni}_2\text{O}_7$, *Phys. Rev. Lett.* **132**, 126503 (2024).

- [54] D.-C. Lu, M. Li, Z.-Y. Zeng, W. Hou, J. Wang, F. Yang, and Y.-Z. You, Superconductivity from doping symmetric mass generation insulators: Application to $\text{La}_3\text{Ni}_2\text{O}_7$ under pressure, [arXiv:2308.11195](https://arxiv.org/abs/2308.11195) (2023).
- [55] J.-X. Zhang, H.-K. Zhang, Y.-Z. You, and Z.-Y. Weng, Strong pairing originated from an emergent \mathbb{Z}_2 berry phase in $\text{La}_3\text{Ni}_2\text{O}_7$, *Phys. Rev. Lett.* **133**, 126501 (2024).
- [56] Z. Pan, C. Lu, F. Yang, and C. Wu, Effect of rare-earth element substitution in superconducting $\text{R}_3\text{Ni}_2\text{O}_7$ under pressure, *Chin. Phys. Lett.* **41** (2024).
- [57] H. Lange, L. Homeier, E. Demler, U. Schollwöck, A. Bohrdt, and F. Grusdt, Pairing dome from an emergent feshbach resonance in a strongly repulsive bilayer model, *Phys. Rev. B* **110**, L081113 (2024).
- [58] H. Yang, H. Oh, and Y.-H. Zhang, Strong pairing from a small Fermi surface beyond weak coupling: Application to $\text{La}_3\text{Ni}_2\text{O}_7$, *Phys. Rev. B* **110**, 104517 (2024).
- [59] H. Schlömer, U. Schollwöck, F. Grusdt, and A. Bohrdt, Superconductivity in the pressurized nickelate $\text{La}_3\text{Ni}_2\text{O}_7$ in the vicinity of a BEC-BCS crossover, *Communications Physics* **7**, 366 (2024).
- [60] H. Lange, L. Homeier, E. Demler, U. Schollwöck, F. Grusdt, and A. Bohrdt, Feshbach resonance in a strongly repulsive ladder of mixed dimensionality: A possible scenario for bilayer nickelate superconductors, *Phys. Rev. B* **109**, 045127 (2024).
- [61] Y. Cao and Y.-f. Yang, Flat bands promoted by hund's rule coupling in the candidate double-layer superconductor with high critical temperature $\text{La}_3\text{Ni}_2\text{O}_7$ under high pressure, *Phys. Rev. B* **109**, L081105 (2024).
- [62] Y. Zhang, L.-F. Lin, A. Moreo, T. A. Maier, and E. Dagotto, Structural phase transition, s_{\pm} -wave pairing, and magnetic stripe order in bilayered superconductor $\text{La}_3\text{Ni}_2\text{O}_7$ under pressure, *Nature Communications* **15**, 2470 (2024).
- [63] B. Geisler, J. J. Hamlin, G. R. Stewart, R. G. Hennig, and P. Hirschfeld, Structural transitions, octahedral rotations, and electronic properties of $\text{A}_3\text{Ni}_2\text{O}_7$ rare-earth nickelates under high pressure, *npj Quantum Mater.* **9**, 38 (2024).
- [64] Y.-H. Tian, Y. Chen, J.-M. Wang, R.-Q. He, and Z.-Y. Lu, Correlation effects and concomitant two-orbital s_{\pm} -wave superconductivity in $\text{La}_3\text{Ni}_2\text{O}_7$ under high pressure, *Phys. Rev. B* **109**, 165154 (2024).
- [65] Z. Luo, B. Lv, M. Wang, W. Wú, and D.-X. Yao, High- T_c superconductivity in $\text{La}_3\text{Ni}_2\text{O}_7$ based on the bilayer two-orbital t-J model, *npj Quantum Mater.* **9**, 61 (2024).
- [66] T. Kaneko, H. Sakakibara, M. Ochi, and K. Kuroki, Pair correlations in the two-orbital Hubbard ladder: Implications for superconductivity in the bilayer nickelate $\text{La}_3\text{Ni}_2\text{O}_7$, *Phys. Rev. B* **109**, 045154 (2024).
- [67] W. Wú, Z. Luo, D.-X. Yao, and M. Wang, Superexchange and charge transfer in the nickelate superconductor $\text{La}_3\text{Ni}_2\text{O}_7$ under pressure, *Sci. China-Phys. Mech. Astron.* **67**, 117402 (2024).
- [68] C. Lu, Z. Pan, F. Yang, and C. Wu, Interplay of two E_g orbitals in superconducting $\text{La}_3\text{Ni}_2\text{O}_7$ under pressure, *Phys. Rev. B* **110**, 094509 (2024).
- [69] J. Chen, F. Yang, and W. Li, Orbital-selective superconductivity in the pressurized bilayer nickelate $\text{La}_3\text{Ni}_2\text{O}_7$: An infinite projected entangled-pair state study, *Phys. Rev. B* **110**, L041111 (2024).
- [70] M. Kakoi, T. Kaneko, H. Sakakibara, M. Ochi, and K. Kuroki, Pair correlations of the hybridized orbitals in a ladder model for the bilayer nickelate $\text{La}_3\text{Ni}_2\text{O}_7$, *Phys. Rev. B* **109**, L201124 (2024).
- [71] Z. Ouyang, M. Gao, and Z.-Y. Lu, Absence of electron-phonon coupling superconductivity in the bilayer phase of $\text{La}_3\text{Ni}_2\text{O}_7$ under pressure, *npj Quantum Materials* **9**, 80 (2024).
- [72] Y. Zhang, L.-F. Lin, A. Moreo, T. A. Maier, and E. Dagotto, Electronic structure, self-doping, and superconducting instability in the alternating single-layer trilayer stacking nickelates $\text{La}_3\text{Ni}_2\text{O}_7$, *Phys. Rev. B* **110**, L060510 (2024).
- [73] G. Heier, K. Park, and S. Y. Savrasov, Competing d_{xy} and s_{\pm} pairing symmetries in superconducting $\text{La}_3\text{Ni}_2\text{O}_7$: LDA + FLEX calculations, *Phys. Rev. B* **109**, 104508 (2024).
- [74] Z. Wang, H.-J. Zhang, K. Jiang, and F.-C. Zhang, Self-doped molecular mott insulator for bilayer superconducting $\text{La}_3\text{Ni}_2\text{O}_7$ with high critical temperature, *National Science Review* **12**, nwfaf353 (2025), <https://academic.oup.com/nsr/article-pdf/12/10/nwfaf353/64110975/nwfaf353.pdf>.
- [75] H.-X. Xu and D. Guterding, Incommensurate spin fluctuations and competing pairing symmetries in $\text{La}_3\text{Ni}_2\text{O}_7$, *Phys. Rev. B* **112**, 174519 (2025).
- [76] S. Rye, N. Witt, and T. O. Wehling, Quenched pair breaking by interlayer correlations as a key to superconductivity in $\text{La}_3\text{Ni}_2\text{O}_7$, *Phys. Rev. Lett.* **133**, 096002 (2024).
- [77] X. Chen, P. Jiang, J. Li, Z. Zhong, and Y. Lu, Charge and spin instabilities in superconducting $\text{La}_3\text{Ni}_2\text{O}_7$, *Phys. Rev. B* **111**, 014515 (2025).
- [78] Y.-Y. Zheng and W. Wú, s_{\pm} -wave superconductivity in the bilayer two-orbital Hubbard model, *Phys. Rev. B* **111**, 035108 (2025).
- [79] C. Xia, H. Liu, S. Zhou, and H. Chen, Sensitive dependence of pairing symmetry on Ni- e_g crystal field splitting in the nickelate superconductor $\text{La}_3\text{Ni}_2\text{O}_7$, *Nat. Commun.* **16**, 1054 (2025).
- [80] T. Kaneko, M. Kakoi, and K. Kuroki, t - J model for strongly correlated two-orbital systems: Application to bilayer nickelate superconductors, *Phys. Rev. B* **112**, 075143 (2025).
- [81] K.-Y. Jiang, Y.-H. Cao, Q.-G. Yang, H.-Y. Lu, and Q.-H. Wang, Theory of pressure dependence of superconductivity in bilayer nickelate $\text{La}_3\text{Ni}_2\text{O}_7$, *Phys. Rev. Lett.* **134**, 076001 (2025).
- [82] E. K. Ko, Y. Yu, Y. Liu, L. Bhatt, J. Li, V. Thampy, C.-T. Kuo, B. Y. Wang, Y. Lee, K. Lee, J.-S. Lee, B. H. Goodge, D. A. Muller, and H. Y. Hwang, Signatures of ambient pressure superconductivity in thin film $\text{La}_3\text{Ni}_2\text{O}_7$, *Nature* **638**, 935 (2025).
- [83] G. Zhou, W. Lv, H. Wang, Z. Nie, Y. Chen, Y. Li, H. Huang, W.-Q. Chen, Y.-J. Sun, Q.-K. Xue, and Z. Chen, Ambient-pressure superconductivity onset above 40 K in $(\text{La,Pr})_3\text{Ni}_2\text{O}_7$ films, *Nature* **640**, 641 (2025).
- [84] Y. Liu, E. K. Ko, Y. Tarn, L. Bhatt, J. Li, V. Thampy, B. H. Goodge, D. A. Muller, S. Raghu, Y. Yu, and H. Y. Hwang, Superconductivity and normal-state transport in compressively strained $\text{La}_2\text{PrNi}_2\text{O}_7$ thin films, *Nature Materials* **24**, 1221 (2025).
- [85] L. Bhatt, A. Y. Jiang, E. K. Ko, N. Schnitzer,

- G. A. Pan, D. F. Segedin, Y. Liu, Y. Yu, Y.-F. Zhao, E. A. Morales, C. M. Brooks, A. S. Botana, H. Y. Hwang, J. A. Mundy, D. A. Muller, and B. H. Goodge, [Resolving structural origins for superconductivity in strain-engineered \$\text{La}_3\text{Ni}_2\text{O}_7\$ thin films](#) (2025), [arXiv:2501.08204 \[cond-mat.supr-con\]](#).
- [86] C. Yue, J.-J. Miao, H. Huang, Y. Hua, P. Li, Y. Li, G. Zhou, W. Lv, Q. Yang, F. Yang, H. Sun, Y.-J. Sun, J. Lin, Q.-K. Xue, Z. Chen, and W.-Q. Chen, Correlated electronic structures and unconventional superconductivity in bilayer nickelate heterostructures, [National Science Review](#) **12**, nwaf253 (2025), <https://academic.oup.com/nsr/article-pdf/12/10/nwaf253/63552132/nwaf253.pdf>.
- [87] M. Osada, C. Terakura, A. Kikkawa, M. Nakajima, H.-Y. Chen, Y. Nomura, Y. Tokura, and A. Tsukazaki, Strain-tuning for superconductivity in $\text{La}_3\text{Ni}_2\text{O}_7$ thin films, [Communications Physics](#) **8**, 251 (2025).
- [88] Q. Li, J. Sun, S. Bötzel, M. Ou, Z.-N. Xiang, F. Lechermann, B. Wang, Y. Wang, Y.-J. Zhang, J. Cheng, I. M. Eremin, and H.-H. Wen, Enhanced superconductivity in the compressively strained bilayer nickelate thin films by pressure, [Nature Communications](#) **10.1038/s41467-026-69660-1** (2026).
- [89] B. Y. Wang, Y. Zhong, S. Abadi, Y. Liu, Y. Yu, X. Zhang, Y.-M. Wu, R. Wang, J. Li, Y. Tarn, E. K. Ko, V. Thampy, M. Hashimoto, D. Lu, Y. S. Lee, T. P. Devereaux, C. Jia, H. Y. Hwang, and Z.-X. Shen, Electronic structure of compressively strained thin film $\text{La}_2\text{PrNi}_2\text{O}_7$, [arXiv:2504.16372](#) (2025).
- [90] B. Hao, M. Wang, W. Sun, Y. Yang, Z. Mao, S. Yan, H. Sun, H. Zhang, L. Han, Z. Gu, J. Zhou, D. Ji, and Y. Nie, Superconductivity in Sr-doped $\text{La}_3\text{Ni}_2\text{O}_7$ thin films, [Nature Materials](#) **24**, 1756 (2025).
- [91] H. Zhong, B. Hao, A. Chen, X. Huang, C. Li, W. Zhang, C. Liu, K. Kummer, N. Brookes, Y. Nie, T. Schmitt, and X. Lu, [Doping evolution of spin excitations in \$\text{La}_{3-x}\text{Sr}_x\text{Ni}_2\text{O}_7/\text{SrLaAlO}_4\$ superconducting thin films](#) (2026), [arXiv:2603.01120 \[cond-mat.supr-con\]](#).
- [92] P. Li, G. Zhou, W. Lv, Y. Li, C. Yue, H. Huang, L. Xu, J. Shen, Y. Miao, W. Song, Z. Nie, Y. Chen, H. Wang, W. Chen, Y. Huang, Z.-H. Chen, T. Qian, J. Lin, J. He, Y.-J. Sun, Z. Chen, and Q.-K. Xue, Angle-resolved photoemission spectroscopy of superconducting $(\text{La},\text{Pr})_3\text{Ni}_2\text{O}_7/\text{SrLaAlO}_4$ heterostructures, [National Science Review](#), nwaf205 (2025).
- [93] J. Shen, G. Zhou, Y. Miao, P. Li, Z. Ou, Y. Chen, Z. Wang, R. Luan, H. Sun, Z. Feng, X. Yong, Y. Li, L. Xu, W. Lv, Z. Nie, H. Wang, H. Huang, Y.-J. Sun, Q.-K. Xue, J. He, and Z. Chen, [Nodeless superconducting gap and electron-boson coupling in \$\(\text{La},\text{Pr},\text{Sm}\)_3\text{Ni}_2\text{O}_7\$ films](#) (2025), [arXiv:2502.17831 \[cond-mat.supr-con\]](#).
- [94] S. Fan, M. Ou, M. Scholten, Q. Li, Z. Shang, Y. Wang, J. Xu, H. Yang, I. M. Eremin, and H.-H. Wen, [Superconducting gap structure and bosonic mode in \$\text{La}_2\text{PrNi}_2\text{O}_7\$ thin films at ambient pressure](#) (2025), [arXiv:2506.01788 \[cond-mat.supr-con\]](#).
- [95] Z. Nie, Y. Li, W. Lv, L. Xu, Z. Jiang, P. Fu, G. Zhou, W. Song, Y. Chen, H. Wang, H. Huang, J. Lin, D. Shen, P. Li, Q.-K. Xue, and Z. Chen, [Ambient-pressure superconductivity and electronic structures of engineered hybrid nickelate films](#) (2025), [arXiv:2509.03502 \[cond-mat.supr-con\]](#).
- [96] F. Li, Z. Xing, D. Peng, J. Dou, N. Guo, L. Ma, Y. Zhang, L. Wang, J. Luo, J. Yang, J. Zhang, T. Chang, Y.-S. Chen, W. Cai, J. Cheng, Y. Wang, Y. Liu, T. Luo, N. Hirao, T. Matsuoka, H. Kadobayashi, Z. Zeng, Q. Zheng, R. Zhou, Q. Zeng, X. Tao, and J. Zhang, Bulk superconductivity up to 96 K in pressurized nickelate single crystals, [Nature](#) **649**, 871 (2026).
- [97] Z. Qiu, J. Chen, D. V. Semenov, Q. Zhong, D. Zhou, J. Li, P. Ma, X. Huang, M. Huo, T. Xie, X. Chen, H. Kwang Mao, V. Struzhkin, H. Sun, and M. Wang, [Interlayer coupling enhanced superconductivity near 100 K in \$\text{La}_{3-x}\text{Nd}_x\text{Ni}_2\text{O}_7\$](#) (2025), [arXiv:2510.12359 \[cond-mat.supr-con\]](#).
- [98] Q. Zhong, J. Chen, Z. Qiu, J. Li, X. Huang, P. Ma, M. Huo, H. Dong, H. Sun, and M. Wang, [Evolution of the superconductivity in pressurized \$\text{La}_{3-x}\text{Sm}_x\text{Ni}_2\text{O}_7\$](#) (2025), [arXiv:2510.13342 \[cond-mat.supr-con\]](#).
- [99] J.-Y. You, Z. Zhu, M. Del Ben, W. Chen, and Z. Li, Unlikelihood of a phonon mechanism for the superconductivity with high critical temperature in $\text{La}_3\text{Ni}_2\text{O}_7$, [npj Computational Materials](#) **11**, 3 (2025).
- [100] R. Khasanov, T. J. Hicken, D. J. Gawryluk, V. Sazgari, I. Plokhikh, L. P. Sorel, M. Bartkowiak, S. Bötzel, F. Lechermann, I. M. Eremin, H. Luetkens, and Z. Guguchia, Pressure-enhanced splitting of density wave transitions in $\text{La}_3\text{Ni}_2\text{O}_{7-\delta}$, [Nature Physics](#) **21**, 430 (2025).
- [101] X. Ren, R. Sutarto, X. Wu, J. Zhang, H. Huang, T. Xiang, J. Hu, R. Comin, X. Zhou, and Z. Zhu, Resolving the electronic ground state of $\text{La}_3\text{Ni}_2\text{O}_{7-\delta}$ films, [Communications Physics](#) **8**, 52 (2025).
- [102] D. Zhao, Y. Zhou, M. Huo, Y. Wang, L. Nie, Y. Yang, J. Ying, M. Wang, T. Wu, and X. Chen, Pressure-enhanced spin-density-wave transition in double-layer nickelate $\text{La}_3\text{Ni}_2\text{O}_{7-\delta}$, [Science Bulletin](#) **70**, 1239 (2025).
- [103] K.-Y. Jiang, Y.-H. Cao, Q.-G. Yang, H.-Y. Lu, and Q.-H. Wang, Theory of pressure dependence of superconductivity in bilayer nickelate $\text{La}_3\text{Ni}_2\text{O}_7$, [Phys. Rev. Lett.](#) **134**, 076001 (2025).
- [104] C. Le, J. Zhan, X. Wu, and J. Hu, [Opposite-mirror-parity scattering as the origin of superconductivity in strained bilayer nickelates](#) (2025), [arXiv:2501.14665 \[cond-mat.supr-con\]](#).
- [105] Y.-H. Cao, K.-Y. Jiang, H.-Y. Lu, D. Wang, and Q.-H. Wang, Strain-engineered electronic structure and superconductivity in $\text{La}_3\text{Ni}_2\text{O}_7$ thin films, [Science China Physics, Mechanics & Astronomy](#) **69**, 247412 (2026).
- [106] S. Ryee, N. Witt, G. Sangiovanni, and T. O. Wehling, Superconductivity governed by janus-faced fermiology in strained bilayer nickelates, [Phys. Rev. Lett.](#) **135**, 236003 (2025).
- [107] Y.-M. Wu, H.-X. Wang, S. V. Smailagić, T. Helbig, and S. Raghu, [Superconductivity and magnetism in bilayer nickelates: itinerant perspective](#) (2026), [arXiv:2602.20288 \[cond-mat.supr-con\]](#).
- [108] Z.-Y. Shao, C. Lu, M. Liu, Y.-B. Liu, Z. Pan, C. Wu, and F. Yang, [Pairing without \$\gamma\$ -pocket in the \$\text{La}_3\text{Ni}_2\text{O}_7\$ thin film](#) (2025), [arXiv:2507.20287 \[cond-mat.supr-con\]](#).
- [109] K. Ushio, S. Kamiyama, Y. Hoshi, R. Mizuno, M. Ochi, K. Kuroki, and H. Sakakibara, [Theoretical study on ambient pressure superconductivity in \$\text{La}_3\text{Ni}_2\text{O}_7\$ thin films : structural analysis, model construction, and robustness of \$s\pm\$ -wave pairing](#) (2025), [arXiv:2506.20497 \[cond-mat.supr-con\]](#).

- [110] C. Lu, M. Zhang, Z. Pan, C. Wu, and F. Yang, Impact of pressure and apical oxygen vacancies on superconductivity in $\text{La}_3\text{Ni}_2\text{O}_7$, *Communications Physics* **8**, 354 (2025).
- [111] M. Bejas, X. Wu, D. Chakraborty, A. P. Schnyder, and A. Greco, Out-of-plane bond-order phase, superconductivity, and their competition in the $t-J_{\parallel}-J_{\perp}$ model: Possible implications for bilayer nickelates, *Phys. Rev. B* **111**, 144514 (2025).
- [112] Y. Yang, X. Lu, Y. Wan, W.-Q. Chen, and S.-S. Gong, Evolution from intralayer to interlayer superconductivity in a bilayer t - J model, [arXiv:2507.07545](https://arxiv.org/abs/2507.07545) (2025).
- [113] Z. Fan, J.-F. Zhang, B. Zhan, D. Lv, X.-Y. Jiang, B. Normand, and T. Xiang, Superconductivity in nickelate and cuprate superconductors with strong bilayer coupling, *Phys. Rev. B* **110**, 024514 (2024).
- [114] J.-H. Ji, C. Lu, Z.-Y. Shao, Z. Pan, F. Yang, and C. Wu, Strong-coupling study of the pairing mechanism in pressurized $\text{La}_3\text{Ni}_2\text{O}_7$, *Phys. Rev. B* **112**, 214515 (2025).
- [115] Z.-Y. Shao, J.-H. Ji, C. Wu, D.-X. Yao, and F. Yang, Possible liquid-nitrogen-temperature superconductivity driven by perpendicular electric field in the single-bilayer film of $\text{La}_3\text{Ni}_2\text{O}_7$ at ambient pressure, *Nature Communications* **17**, 1120 (2026).
- [116] H. Lange, A. Chen, A. Georges, F. Grusdt, A. Bohrdt, and C. Roth, *Simulating superconductivity in mixed-dimensional $t_{\parallel}-J_{\parallel}-J_{\perp}$ bilayers with neural quantum states* (2026), [arXiv:2602.10091](https://arxiv.org/abs/2602.10091) [cond-mat.str-el].
- [117] Z.-D. Fan and A. Vishwanath, *Minimal two band model and experimental proposals to distinguish pairing mechanisms of the high- T_c superconductor $\text{La}_3\text{Ni}_2\text{O}_7$* (2025), [arXiv:2512.05956](https://arxiv.org/abs/2512.05956) [cond-mat.str-el].
- [118] G. Zhou, H. Wang, H. Huang, Y. Chen, F. Peng, W. Lv, Z. Nie, W. Wang, J.-F. Jia, Q.-K. Xue, and Z. Chen, Superconductivity onset above 60 K in ambient-pressure nickelate films, *National Science Review*, nwag151 (2026), <https://academic.oup.com/nsr/advance-article-pdf/doi/10.1093/nsr/nwag151/67287664/nwag151.pdf>.
- [119] Y. Liu, B. Y. Wang, J. Li, Y. Tarn, L. Bhatt, M. Colletta, Y.-M. Wu, C.-T. Kuo, J.-S. Lee, B. H. Goodge, D. A. Muller, Z.-X. Shen, S. Raghu, H. Y. Hwang, and Y. Yu, *A superconducting half-dome in bilayer nickelates* (2026), [arXiv:2603.12196](https://arxiv.org/abs/2603.12196) [cond-mat.supr-con].
- [120] Y. Tian and Y. Chen, Spin density wave and superconductivity in the bilayer t - J model of $\text{La}_3\text{Ni}_2\text{O}_7$ under renormalized mean-field theory, *Phys. Rev. B* **112**, 014520 (2025).
- [121] Z. Chen, Y.-B. Liu, and F. Yang, *Variation monte carlo study on the bilayer $t - J_{\parallel} - J_{\perp}$ model for $\text{La}_3\text{Ni}_2\text{O}_7$* (2025), [arXiv:2510.04224](https://arxiv.org/abs/2510.04224) [cond-mat.supr-con].
- [122] G. Kotliar and J. Liu, Superexchange mechanism and d-wave superconductivity, *Phys. Rev. B* **38**, 5142 (1988).
- [123] P. A. Lee, N. Nagaosa, and X.-G. Wen, Doping a mott insulator: Physics of superconductivity with high critical temperature, *Rev. Mod. Phys.* **78**, 17 (2006).
- [124] S. R. White, Density-matrix algorithms for quantum renormalization groups, *Phys. Rev. B* **48**, 10345 (1993).
- [125] Jutho, L. Devos, M. Hauru, maartenvd, ho oto, Gertian, L. Burgelman, tangwei94, J. TagBot, S. Carlström, V. Vanthilt, Xiaoyu, and qmortier, [Jutho/tensorkit.jl: v0.12.7](https://github.com/Jutho/tensorkit.jl) (2024).
- [126] Q. Li, [FiniteMPS.jl](https://github.com/q-li/FiniteMPS.jl) (2025).
- [127] A. Weichselbaum, Non-abelian symmetries in tensor networks: A quantum symmetry space approach, *Ann. Phys.* **327**, 2972 (2012).
- [128] A. Weichselbaum, X-symbols for non-abelian symmetries in tensor networks, *Phys. Rev. Res.* **2**, 023385 (2020).
- [129] Y. Chen, Y.-H. Tian, J.-M. Wang, R.-Q. He, and Z.-Y. Lu, Non-fermi liquid and antiferromagnetic correlations with hole doping in the bilayer two-orbital hubbard model of $\text{La}_3\text{Ni}_2\text{O}_7$ at zero temperature, *Phys. Rev. B* **110**, 235119 (2024).
- [130] Z. Ouyang, J.-M. Wang, J.-X. Wang, R.-Q. He, L. Huang, and Z.-Y. Lu, Hund electronic correlation in $\text{La}_3\text{Ni}_2\text{O}_7$ under high pressure, *Phys. Rev. B* **109**, 115114 (2024).
- [131] C.-Q. Chen, W. Qiu, Z. Luo, M. Wang, and D.-X. Yao, Electronic structures and superconductivity in ndoped $\text{La}_3\text{Ni}_2\text{O}_7$, *Science China Physics, Mechanics & Astronomy* **69**, 247414 (2026).
- [132] W.-Y. Chen, C.-Q. Chen, M. Wang, S.-S. Gong, and D.-X. Yao, *Superconductivity of bilayer two-orbital hubbard model for $\text{La}_3\text{Ni}_2\text{O}_7$ under high pressure* (2025), [arXiv:2511.01801](https://arxiv.org/abs/2511.01801) [cond-mat.supr-con].
- [133] X.-W. Yi, W. Li, J.-Y. You, B. Gu, and G. Su, Unifying strain- and pressure-driven superconductivity in $\text{La}_3\text{Ni}_2\text{O}_7$: Suppressed charge and spin density waves and enhanced interlayer coupling, *Phys. Rev. B* **112**, L140504 (2025).
- [134] X.-W. Yi, Y. Meng, J.-W. Li, Z.-W. Liao, W. Li, J.-Y. You, B. Gu, and G. Su, Nature of charge density waves and metal-insulator transition in pressurized $\text{La}_3\text{Ni}_2\text{O}_7$, *Phys. Rev. B* **110**, L140508 (2024).
- [135] Y. Tarn, Y. Liu, F. Theuss, J. Li, B. Y. Wang, L. Bhatt, J. Wang, J. Song, V. Thampy, B. H. Goodge, D. A. Muller, Z.-X. Shen, Y. Yu, and H. Y. Hwang, Reducing the strain required for ambient-pressure superconductivity in ruddlesden-popper bilayer nickelates, *Advanced Materials* **n/a**, e20724.
- [136] B. Geisler, J. J. Hamlin, G. R. Stewart, R. G. Hennig, and P. J. Hirschfeld, Electronic reconstruction and interface engineering of emergent spin fluctuations in compressively strained $\text{La}_3\text{Ni}_2\text{O}_7$ on $\text{SrLaAlO}_4(001)$, *Phys. Rev. B* **113**, 054516 (2026).
- [137] X. Hu, W. Qiu, C.-Q. Chen, Z. Luo, and D.-X. Yao, Electronic structures and multi-orbital models of $\text{La}_3\text{Ni}_2\text{O}_7$ thin films at ambient pressure, *Communications Physics* **8**, 10.1038/s42005-025-02411-8 (2025).
- [138] S. Bheemavarapu, *Strain-tuned structural, electronic, and superconducting properties of thin-film $\text{La}_3\text{Ni}_2\text{O}_7$* (2025), [arXiv:2512.23630](https://arxiv.org/abs/2512.23630) [cond-mat.supr-con].
- [139] Z.-Y. Shao, Y.-B. Liu, M. Liu, and F. Yang, Band structure and pairing nature of $\text{La}_3\text{Ni}_2\text{O}_7$ thin film at ambient pressure, *Phys. Rev. B* **112**, 024506 (2025).
- [140] H. C. R. B. Bhatta, X. Zhang, Y. Zhong, and C. Jia, *Structural and electronic evolution of bilayer nickelates under biaxial strain* (2025), [arXiv:2502.01624](https://arxiv.org/abs/2502.01624) [cond-mat.supr-con].
- [141] Y.-F. Zhao and A. S. Botana, Electronic structure of ruddlesden-popper nickelates: Strain to mimic the effects of pressure, *Phys. Rev. B* **111**, 115154 (2025).
- [142] Z. Dong, G. Wang, N. Wang, W.-H. Dong, L. Gu, Y. Xu, J. Cheng, Z. Chen, and Y. Wang, Interstitial oxygen order and its competition with superconductivity in $\text{La}_2\text{PrNi}_2\text{O}_{7+\delta}$, *Nature Materials* **24**, 1927 (2025).
- [143] Z. Zhang, M. Greenblatt, and J. Goodenough, Synthesis, structure, and properties of the layered perovskite

- $\text{La}_3\text{Ni}_2\text{O}_{7-\delta}$, [Journal of Solid State Chemistry](#) **108**, 402 (1994).
- [144] J. Shen, Y. Miao, Z. Ou, G. Zhou, Y. Chen, R. Luan, H. Sun, Z. Feng, X. Yong, P. Li, Y. Li, L. Xu, W. Lv, Z. Nie, H. Wang, H. Huang, Y.-J. Sun, Q.-K. Xue, Z. Chen, and J. He, Anomalous energy gap in superconducting $\text{La}_{2.85}\text{Pr}_{0.15}\text{Ni}_2\text{O}_7/\text{SrLaAlO}_4$ heterostructures, [arXiv:2502.17831](#) (2025).
- [145] Y. L. Lee, Y. W. Lee, C.-Y. Mou, and Z. Y. Weng, Two-leg t-J ladder: A mean-field description, [Phys. Rev. B](#) **60**, 13418 (1999).